Revista Mexicana de Astronomía y Astrofísica, **39**, 149–170 (2003)

INFRARED IMAGING AND OPTICAL IMAGING AND SPECTROSCOPY OF (MOSTLY) TYPE I PLANETARY NEBULAE II.[1]

J. Bohigas

Instituto de Astronomía
Universidad Nacional Autónoma de México, Ensenada, B. C., México

Received 2003 January 8; accepted 2003 April 1

RESUMEN

Se presentan datos espectroscópicos, imágenes en las principales líneas ópticas de emisión e imágenes infrarrojas para descubrir la presencia de hidrógeno molecular, de 14 nebulosas planetarias (NPs). Once de éstas satisfacen los dos criterios que definen a las NPs de tipo I (ricas en helio con un alto cociente N/O). Todas son clasificadas como bipolares, aunque dos de ellas (A 24 y M 3-5) pudieran ser bipolares vistas de frente o elípticas. Hidrógeno molecular chocado está presente en ocho de estos objetos, pero no en A 14, A 24 y M 1-57. KjPn 6 fue tentativamente clasificada como de tipo I, aunque su abundancia de helio es menor que el valor prescrito y la suma de las abundancias de nitrógeno y oxígeno es baja. Este objeto está a unos 800 pc del plano galáctico, es bipolar y no contiene hidrógeno molecular. La composición química de A 24, A 79, M 1-57 y Sh 1-89 indica que se produjeron episodios de tercer dragado en su estrella progenitora. Se encontró evidencia de choques en la componente ionizada de A 79, M 1-28 y NGC 2818, y posiblemente A 14, A 24 y K 3-46. Un arco de emisión en la periferia de Wray 16-22, una NP de tipo III, puede interpretarse como un choque de proa debido al movimiento supersónico de este objeto en el medio interestelar.

ABSTRACT

Optical spectra, images in the main optical emission lines and IR images directed towards the detection of molecular hydrogen, were obtained for 14 planetary nebulae (PNe). Eleven of these comply with the two criteria defining a type I PNe (He-rich with a large N/O ratio). All are classified as bipolar, though two of them (A 24 and M 3-5) are either bipolars seen pole-on or elliptical. Shocked molecular hydrogen was detected in eight of these objects, but not in A 14, A 24, and M 1-57. KjPn 6 was tentatively classified as a type I PN, though its helium abundance is smaller than the minimum prescribed value and the sum of its nitrogen and oxygen abundances is low. The object is about 800 pc above the galactic plane, is bipolar and shows no trace of molecular hydrogen. The chemical composition of A 24, A 79, M 1-57, and Sh 1-89 indicates that third dredge-up episodes occured in their progenitor star. Shock waves are propagating in the ionized component of A 79, M 1-28 and NGC 2818, and possibly A 14, A 24, and K 3-46. An emission arc in the periphery of Wray 16-22, a type III PN, may be interpreted as a bow shock produced by the supersonic motion of this object in the interstellar medium.

Key Words: **ISM: INDIVIDUAL (A 24: A 79: KJPN 6: M 3-3: SH 1-89: WRAY 16-22) — ISM: PLANETARY NEBULAE**

1. INTRODUCTION

Peimbert & Torres-Peimbert (1983) defined type I planetary nebulae (PNe) as those where He/H $\geq$ 0.125 *and* N/O $\geq$ 0.5. These large abundances can

[1]Based on observations collected at the Observatorio Astronómico Nacional in San Pedro Mártir, B. C., México.

only be produced by the most massive stars ejecting PNe, i.e., those where the ZAMS mass is between ~ 2.5 and $8\,M_\odot$ (Iben 1995). In a recent paper Bohigas (2001, henceforth BJ) presented infrared imaging and optical imaging and spectroscopy of 14 PNe. Eleven of these were found to be type I. This is the second part of this program. Optical spectra, images in the main optical emission lines and IR images directed towards the detection of molecular hydrogen, were obtained for an additional 14 PNe: A 14, A 24, A 79, DeHt 3, K 3-46, K 3-91, KjPn 6, M 1-28, M 1-57, M 3-3, M 3-5, NGC 2818, Sh 1-89, and Wray 16-22. These were chosen from the *Strasbourg-ESO Catalogue of Planetary Nebulae* (Acker et al. 1992) based on relatively large intensities of [N II] 6584 and/or [S II] 6724 with respect to Hα. This paper is organized as follows: the experimental setup and data reduction procedures are described in § 2, observations are discussed in some detail in § 3, and the last section summarizes the most significant findings.

2. OBSERVATIONS AND DATA REDUCTION

2.1. *Optical Imaging*

Images with narrow band filters centered at Hβ, [O III] 5007, Hα, [N II] 6584, and [S II] 6724 were obtained for most of the objects discussed in this paper. The SPM set of nebular filters (series I and II) was used. Filter properties can be found at `http://bufadora.astrosen.unam.mx/Instruments/filtros/filtros.html` (Bohigas 1990). Images were secured in several observing runs using the 1.5 and 0.84 m telescopes at the Observatorio Astronómico Nacional at San Pedro Mártir, B.C., México (OAN) and various CCD detectors. The *RUCA* filter wheel (Zazueta et al. 2000) was used in these observations. Integration times are typically 20 minutes. Sky flats were used in all these runs. Image quality was rarely better than 1.3″. The Hα images were used to determine the total Hα flux from each object in the manner described in BJ. Images of these objects in some of the emission lines explored in this work have been reported in a number of contributions, among them *The IAC Morphological Catalog of Northern Galactic Planetary Nebulae* (Manchado et al. 1996, henceforth IAC-Catalog).

2.2. *IR Imaging*

Infrared images were obtained with the *H2* ($\lambda_0 = 2.122\,\mu$m, FWHM $= 0.02\,\mu$m) and *cK* ($\lambda_0 = 2.26\,\mu$m, FWHM $= 0.06\,\mu$m) filters of the CAMILA imaging system (Cruz-González et al. 1994) attached to the 2.1 m f/13.5 telescope of the OAN. The field of view of the detector, a NICMOS3 256×256 pixel^2 infrared camera, is $218'' \times 218''$. Image quality is 2–3 pixel in all cases. Typical total integration times are 900 s for *H2*, and 600 s for *cK*. Most objects are completely included in a quadrant of the detector, and were rastered to different locations within it. In these cases the sky frame is the median of all images in the sequence (more than 9). For large objects the sky frame was produced from images in the immediate vicinity. Flat fields are the median of all night frames for each filter. Since detection and morphology were the main goals in the IR band, the images are not photometrically calibrated. An ample discussion on the filter properties and procedure followed to determine the presence of shock excited H_2 can be found in BJ. The presence of shocked molecular hydrogen has already been reported by Kastner et al. (1996, henceforth KWGMP) in A 79, K 3-46, M 1-28, and Sh 1-89.

2.3. *Optical Spectroscopy*

Spectroscopy was carried out with the Boller & Chivens spectrograph at the 2.1 m f/7.5 telescope of the OAN. A 600 lines mm^{-1} grating blazed at 4550 Å was used to cover the 3700–5300 and 4750–6850 Å wavelength intervals. In ten cases a 600 lines mm^{-1} grating blazed at 6825 Å was used to cover the 6600–8700 Å wavelength interval. The slit was 250 μm wide and its alignment varied from object to object (see Table 1). The mean spectral resolution and dispersion are ~ 3 pixel and 2.05 Å/pixel, respectively (the pixel size is 24 μm). Most exposures were 20 minutes long. Flux calibration was performed and crosschecked using several standard stars.

Data reduction was performed applying IRAF[2] standard procedures. Most extraction apertures are $5'' \times 3''$ (length and width of the slit). To obtain a higher signal to noise ratio, a larger aperture was used for A 14, A 24, and KjPn 6 (see Tables 2a and 2b). Sky spectra were extracted from the same frame as the object spectra. The positions at which the latter were obtained (accurate within 2″) are annotated in Table 1, and are given in relation to stars from the Hubble Guide Star Catalogue (also listed in this table) or the central star of the PN (listed as PNN). These positions are marked in one of the optical images of each object (Figures 1 to 16). References to previous spectroscopic observations are also included in Table 1 (under Other).

Line fluxes relative to Hβ (100 in all cases) are reported in Tables 2a, 2b, and 2c. Errors in the

[2] IRAF is distributed by NOAO which is operated by AURA under contract to the NSF.

TABLE 1

SPECTRAL POSITIONS

Object	Name	GSC	$\Delta\alpha$	$\Delta\delta$	PA	Other[a]
G197.8-03.3	A 14	PNN	$0''$	$0''$	NS	
G217.1+14.7	A 24	0184-00791	$-36''$	$121''$	NS	
G102.9-02.3	A 79	3986-02726	$-24''$	$-53''$	NS	RCM
G019.4-13.6	DeHt 3	6300-00675	$-43''$	$-23''$	EW	
G069.2+03.8	K 3-46	2677-00096	$79''$	$-16''$	NS	
G129.5+04.5	K 3-91	4044-00266	$107''$	$125''$	EW	
G111.2+07.0	KjPn 6	4277-00986	$-53''$	$-45''$	NS	KPP
G006.0+03.1	M 1-28	6261-01631	$5''$	$115''$	NS	AKSR
G022.1-02.4	M 1-57	PNN	$0''$	$0''$	NS	AKSJ, MKHC
G221.7+05.3	M 3-3	4825-00410	$35''$	$43''$	EW	KB, KSK, PTP
G245.4+01.6	M 3-5	6562-01266	$52''$	$-96''$	NS	KB, KKSB
G261.9+08.5	NGC 2818	7164-03987	$-72''$	$20''$	EW	DU, PTP
G089.8-00.6	Sh 1-89	3593-03813	$-107''$	$-30''$	NS	KSK, SFO
G255.7+03.3	Wray 16-22	7144-03285	$-2''$	-45$''$	EW	

[a]Other spectroscopic work by: AKSJ: Acker et al. 1989. AKSR: Acker et al. 1991. DU: Dufour 1984. KB: Kingsburgh & Barlow 1994. KKSB: Kaler et al. 1996. KPP: Kazarian et al. 1998. KSK: Kaler et al.1990. MKHC: Milingo et al. 2002. PTP: Peimbert & Torres-Peimbert 1987. RCM: Rodríguez et al. 2001. SFO: Sabbadin et al. 1987.

Hβ fluxes are always smaller than 15%. The red spectrum was scaled using Hα. Reddening corrections were performed with Seaton's (1979) extinction law assuming that Hα/Hβ = 2.8. Electron densities and temperatures were determined using the *nebular* package from the Space Telescope Science Data Analysis System. These parameters are given in Table 3. The S^+ lines are very well defined in all cases, and ratios are probably precise at the $\sim$ 5% level. Temperatures ($T(O^{+2})$ and $T(N^+)$) were determined from the $R(O^{+2})$ = [O III] $(4959 + 5007)/4363$ and $R(N^+)$ = [N II] $(6548 + 6584)/5755$ line ratios. Upper and lower bounds for the nitrogen and oxygen temperatures were determined assuming that the corresponding line ratios are uncertain at the 10% level when the flux of the weakest line involved in the ratio ([N II] 5755 or [O III] 4363) is larger than $5 \times 10^{-16}\,\mathrm{erg\,cm^{-2}\,s^{-1}}$, and at the 20% level when smaller than this quantity.

Ion abundances are presented in Table 4. The abundance of helium ions was calculated following Aller (1984). Collisional effects on the He I lines were always considered when determining the He^+ abundance (Kingdon & Ferland 1995). All other ion concentrations were computed with the *nebular* package. Ion concentrations were calculated as in BJ. In A 14, A 24, K 3-46, K 3-91, and KjPn 6 it was not possible to determine the electron temperature from the oxygen lines. Since $T(O^{+2}) > T(N^+)$ in most planetary nebulae, the respective ion concentrations for these objects were determined with a very simple assumption, i.e., $T(O^{+2}) = T(N^+) + 1000$ K. The oxygen temperature can be estimated from the nitrogen temperature and the intensity of He II 4686 (e.g., Kaler 1986; Kingsburgh & Barlow 1994, henceforth KB). Abundances in A 14, A 24, K 3-46, and K 3-91 were also explored using the empirical relation found by KB.

Elemental abundances are also presented in Tables 4a and 4b. The total helium abundance was determined from the concentrations of He^+ and He^{+2} derived from He I 5876 and He II 4686. Abundances from all the other elements were computed using the ionization correction factors given by KB. When available, oxygen abundances were derived using the O^+ concentration from [O II] 3727. In A 14 and KjPn 6 no O^+ line was detected, and abundances were determined using the upper limit for the O^+/H^+ ratio.

3. DISCUSSION

3.1. *General Properties*

A summary of some of the properties of these objects is presented in Table 5. The logarithm of the total Hα flux (F_α, not corrected for reddening) was

TABLE 2

SPECTRAL RESULTS (Hβ = 100)

	A 14[d]		A 24[e]		A 79		DeHt 3		K 3-46	
ID	F_λ	I_λ	F_λ	I_λ	F_λ	I_λ	F_λ	I_λ	F_λ	I_λ
[O II] 3727	···	···	217	244	407	528	648	689	209	402
[Ne III] 3869	···	···	78.9	87.6	128	159	93.0	98.1	60.5	106
Hδ	···	···	27.4	29.6	26.3	31.1	30.1	31.3	12.5	19.1
Hγ	30.6	41.0	45.6	51.7	43.7	51.0	49.0	50.5	34.9	47.9
[O III] 4363	···	···	···	···	8.27	9.35	8.50	8.75	···	···
He I 4471	···	···	11.9	12.4	6.63	7.28	···	···	···	···
He II 4686	30.7	33.7	23.9	24.3	46.9	48.8	26.7	27.0	19.3	21.3
[Ar IV] 4711[a]	···	···	···	···	···	···	···	···	···	···
[Ne IV] 4725	···	···	···	···	···	···	···	···	···	···
[Ar IV] 4740	···	···	···	···	···	···	···	···	···	···
[O III] 4959	104	98.5	52.5	52.0	153	150	278	277	120	113
[O III] 5007	332	307	157	154	457	443	840	833	371	341
[N I] 5200	34.0	28.8	22.4	21.6	37.2	34.7	3.19	3.14	30.5	25.4
[Cl III] 5518	···	···	···	···	···	···	···	···	···	···
[Cl III] 5538	···	···	···	···	···	···	···	···	···	···
[N II] 5755	44.7	29.0	18.2	16.6	42.5	35.4	4.44	4.25	46.2	28.8
He I 5876	25.4	15.6	38.7	35.0	32.3	26.3	15.3	14.6	38.4	22.6
[O I] 6300 ···	···	···	···	166	126	29.2	27.3	63.0	31.2	
[S III] 6312 ···	···	···	···	···	···	···	······	···		
[O I] 6364	···	···	···	···	56.1	42.2	9.30	8.69	22.8	11.0
[Ar V] 6435	···	···	···	···	···	···	···	···	···	···
[N II] 6548	990	479	625	539	881	646	94.6	87.9	1252	567
Hα	581	280	325	280	383	280	302	280	620	280
[N II] 6584	2993	1435	1772	1528	2843	2076	282	262	3884	1744
He I 6678	7.86	3.66	11.5	9.87	13.8	9.95	4.01	3.71	14.8	6.42
[S II] 6717	125	57.1	62.3	53.4	194	139	32.4	30.0	227	97.6
[S II] 6731	93.6	42.9	44.0	37.6	157	113	24.2	22.4	167	71.2
[Ar V] 7006	···	···	···	···	···	···	···	···	···	···
He I 7065	···	···	···	···	9.23	6.37 ···	···	9.15	3.56	
[Ar III] 7136	47.1	19.5	30.0	25.0	46.7	32.0 ···	···	81.5	31.1	
He II 7178	···	···	···	···	···	···	···	···	···	···
[O II] 7320	···	···	···	···	19.6	13.2 ···	···	18.4	6.72	
[O II] 7331	···	···	···	···	18.5	12.4 ···	···	11.1	4.04	
[Ar III] 7751	···	···	···	···	12.1	7.80 ···	···	24.4	8.03	
F(Hβ)[b]	0.59	···	2.31	···	0.77	···	1.98	···	0.39	···
C(Hβ)	0.98	···	0.20	···	0.42	···	0.10	···	1.07	···
I(Hβ)[c]	···	0.57	···	0.36	···	0.20	···	0.25	···	0.45

[a]Blend [Ar IV] 4711, He I 4713, and [Ne IV] 4715. [b]F(Hβ) in 10^{-14} erg cm^{-2} s^{-1}. [c]I(Hβ) in 10^{-13} erg cm^{-2} s^{-1}.
[d]A 14 aperture is 23$''$ long. [e]A 24 aperture is 21$''$ long.

TABLE 2 (CONTINUED)

	K 3-91		KjPn 6[d]		M 1-28		M 1-57		M 3-3	
ID	F_λ	I_λ	F_λ	I_λ	F_λ	I_λ	F_λ	I_λ	F_λ	I_λ
[O II] 3727	···	···	···	···	115	246	66.1	205	169	308
[Ne III] 3869	···	···	···	···	61.3	118	66.0	175	41.9	70.5
Hδ	···	···	11.6	20.6	13.7	22.5	11.8	24.5	16.2	24.0
Hγ	···	···	30.0	46.0	33.3	48.1	28.4	49.2	37.0	49.6
[O III] 4363	···	···	···	···	7.21	10.3	20.4	34.7	5.36	7.09
He I 4471	···	···	2.89	3.97	···	···	2.17	3.25	5.05	6.23
He II 4686	64.3	79.0	···	···	34.1	38.3	44.8	53.4	14.5	15.9
[Ar IV] 4711[a]	···	···	···	···	4.26	4.73	6.08	7.08	···	···
[Ne IV] 4725	···	···	···	···	···	···	2.29	2.58	···	···
[Ar IV] 4740	···	···	···	···	3.62	3.91	9.62	10.8	···	···
[O III] 4959	519	463	32.4	30.0	229	214	705	639	262	249
[O III] 5007	1720	1450	106	94.5	717	650	2309	1997	844	781
[N I] 5200	···	···	1.13	0.89	25.7	20.8	4.63	3.39	25.5	21.6
[Cl III] 5518	···	···	···	···	2.86	1.92	1.52	0.84	···	···
[Cl III] 5538	···	···	···	···	3.07	2.03	2.72	1.48	···	···
[N II] 5755	28.5	10.9	4.10	2.18	35.0	20.3	28.2	12.5	25.8	16.7
He I 5876	42.5	14.3	33.2	16.2	24.8	13.4	31.7	12.6	26.4	16.2
[O I] 6300	125	29.7	···	···	37.1	16.4	106	31.4	45.9	24.0
[S III] 6312	···	···	···	···	14.0	6.16	28.7	8.44	···	···
[O I] 6364	41.6	9.45	···	···	15.4	6.62	35.3	10.1	15.2	7.81
[Ar V] 6435	···	···	···	···	···	···	7.39	2.06	···	···
[N II] 6548	874	172	287	99.1	1056	421	491	125	825	399
Hα	1426	280	818	280	707	280	1109	280	582	280
[N II] 6584	2789	528	900	307	3351	1320	1502	376	2650	1268
He I 6678	22.1	4.02	10.6	3.47	9.21	3.50	11.2	2.64	8.49	3.94
[S II] 6717	48.2	8.56	16.3	5.23	160	59.7	92.2	21.4	17.7	8.12
[S II] 6731	54.2	9.52	16.7	5.31	160	59.4	159	36.6	14.6	6.69
[Ar V] 7006	···	···	···	···	···	···	···	···	···	···
He I 7065	12.6	1.82	···	···	11.3	3.77	···	···	11.7	4.90
[Ar III] 7136	135	18.9	···	···	99.6	33.2	···	···	43.3	17.9
He II 7178	···	···	···	···	3.34	1.09	···	···	···	···
[O II] 7320	46.4	5.84	···	···	14.6	4.51	···	···	8.59	3.40
[O II] 7331	40.1	5.05	···	···	10.8	3.34	···	···	10.7	4.22
[Ar III] 7751	49.4	5.08	···	···	29.2	8.02	···	···	15.3	4.83
F(Hβ)[b]	0.13	···	7.34	···	1.49	···	17.2	···	2.59	···
C(Hβ)	2.19	···	1.44	···	1.24	···	1.85	···	0.98	···
I(Hβ)[c]	···	2.09	···	20.2	···	2.61	···	122	···	2.51

[a]Blend [Ar IV] 4711, He I 4713, and [Ne IV] 4715. [b]F(Hβ) in 10^{-14} erg cm^{-2} s^{-1}. [c]I(Hβ) in 10^{-13} erg cm^{-2} s^{-1}.
[d]KjPn 6 aperture is 11$''$ long.

TABLE 2 (CONTINUED)

	M 3-5		NGC 2818		Sh 1-89		Wray 16-22	
ID	F_λ	I_λ	F_λ	I_λ	F_λ	I_λ	F_λ	I_λ
[O II] 3727	131	205	451	523	221	421	203	300
[Ne III] 3869	70.0	103	140	159	64.1	112	60.4	84.3
Hδ	17.6	23.5	24.4	26.8	16.5	25.1	19.8	25.5
Hγ	40.0	49.7	45.3	48.7	33.6	45.9	38.5	46.4
[O III] 4363	12.9	16.0	13.8	14.8	3.06	4.13	8.49	10.2
He I 4471	3.87	4.54	4.21	4.44	3.82	4.81	3.71	4.27
He II 4686	35.0	37.5	32.3	33.0	23.4	25.9	9.98	10.6
[Ar IV] 4711[a]	3.29	3.49	···	···	···	···	···	···
[Ne IV] 4725	···	···	···	···	···	···	···	···
[Ar IV] 4740	2.26	2.36	···	···	···	···	···	···
[O III] 4959	372	358	265	262	225	213	281	272
[O III] 5007	1155	1091	821	805	722	665	869	827
[N I] 5200	5.69	5.03	22.8	21.9	15.8	13.2	···	···
[Cl III] 5518	0.75	0.59	···	···	···	···	···	···
[Cl III] 5538	0.84	0.66	···	···	···	···	···	···
[N II] 5755	12.1	8.79	21.1	19.0	11.3	7.14	2.63	1.98
He I 5876	19.2	13.3	17.7	15.7	31.5	18.6	14.0	10.2
[O I] 6300	28.4	17.6	53.5	45.7	89.2	44.6	17.8	11.7
[S III] 6312	1.54	0.95	3.22	2.74	···	···	3.18	2.09
[O I] 6364	9.10	5.55	17.7	15.1	28.1	13.8	6.32	4.11
[Ar V] 6435	···	···	···	···	···	···	···	···
[N II] 6548	213	126	440	369	529	243	45.7	28.6
Hα	482	280	335	280	614	280	449	280
[N II] 6584	663	383	1363	1138	1676	761	137	85.0
He I 6678	6.17	3.49	5.67	4.70	12.1	5.30	4.69	2.86
[S II] 6717	13.8	7.75	134	110	105	45.8	47.2	28.5
[S II] 6731	15.3	8.55	96.5	79.7	89.0	35.5	35.1	21.2
[Ar V] 7006	0.82	0.44	···	···	···	···	···	···
He I 7065	8.69	4.57	···	···	4.52	1.78 ···	···	
[Ar III] 7136	38.4	19.9	37.8	30.4	37.2	14.4	···	···
He II 7178	···	···	···	···	···	···	···	···
[O II] 7320	19.6	9.86	14.7	11.7	4.61	1.70	···	···
[O II] 7331	12.9	6.47	15.0	12.0	5.02	1.85	···	···
[Ar III] 7751	9.67	4.53	···	···	12.5	4.19	···	···
$F(\mathrm{H}\beta)$[b]	30.0	···	3.94	···	0.93	···	3.53	···
$C(\mathrm{H}\beta)$	0.73	···	0.24	···	1.06	···	0.64	···
$I(\mathrm{H}\beta)$[c]	···	16.1	···	0.69	···	1.06	···	1.53

[a]Blend [Ar IV] 4711, He I 4713, and [Ne IV] 4715. [b]$F(\mathrm{H}\beta)$ in 10^{-14} erg cm^{-2} s^{-1}. [c]$I(\mathrm{H}\beta)$ in 10^{-13} erg cm^{-2} s^{-1}.

TABLE 3

DENSITY AND TEMPERATURE

Object	R([S II])[a]	N_e	R([N II])	$T_e(N^+)$	R([O III])[b]	$T_e(O^{+2})$
A 14	1.33	85^{+70}_{-60}	65.9	12000^{+600}_{-500}	...	...
A 24	1.42	15^{+60}_{-15}	124	9200^{+400}_{-300}	...	...
A 79	1.23	200^{+90}_{-70}	76.9	11100^{+600}_{-400}	63.4	15600^{+900}_{-600}
DeHt 3	1.34	80^{+70}_{-60}	82.4	10800^{+500}_{-400}	128	11700^{+500}_{-300}
K 3-46	1.37	50^{+70}_{-50}	80.2	10900^{+600}_{-400}	...	...
K 3-91	0.90	970^{+220}_{-170}	64.2	11900^{+1500}_{-1000}	...	...
KjPn 6	0.98	600^{+140}_{-110}	186	7900^{+300}_{-200}	...	...
M 1-28	1.01	590^{+140}_{-110}	85.8	10500^{+600}_{-400}	83.9	13800^{+600}_{-500}
M 1-57	0.59	5300^{+1600}_{-1100}	40.3	14100^{+900}_{-800}	76.0	14300^{+700}_{-600}
M 3-3	1.21	230^{+80}_{-80}	99.8	9900^{+400}_{-300}	145	11200^{+500}_{-300}
M 3-5	0.91	970^{+220}_{-180}	57.9	12600^{+700}_{-600}	90.6	13400^{+600}_{-500}
NGC 2818	1.39	35^{+65}_{-35}	79.3	11000^{+500}_{-500}	72.1	14700^{+800}_{-600}
Sh 1-89	1.29	130^{+70}_{-60}	141	8800^{+300}_{-300}	213	9900^{+800}_{-500}
Wray 16-22	1.35	65^{+80}_{-65}	57.3	12900^{+700}_{-600}	108	12500^{+500}_{-400}

[a] R([S II]) = [S II] 6717/6731; R([N II]) = [N II] (6548+6584)/5755. [b] R([O III]) = [O III] (4959+5007)/4363.

derived from the flux calibrated Hα images obtained for each object. The mass of ionized hydrogen was determined in the manner prescribed by BJ. The large error bars are largely due to the generous allowance made on variations in $C(\mathrm{H}\beta)$ (a 30% variation on the number given in Table 2). The temperature and visual magnitude (not corrected for reddening) of central stars were calculated using the simple formulae given by Kaler & Jacoby (1989) for optically thick PNe. According to these authors optically thick PNe are those where [O II] 3727/H$\beta \geq 1$ (corrected for reddening), but BJ finds that the lower limit should be at least twice as large. The Zanstra temperature and visual magnitude of central stars are given in Table 5 under the columns labelled T_c and V_o. Errors in the visual magnitudes take into account the estimated precision of the spectral data and variations in the value of C(Hβ). The Zanstra temperature is used in combination with theoretical evolutionary tracks for hydrogen burning PNN produced by Vassiliadis & Wood (1994, henceforth VW94) and Blöcker (1995, henceforth BL95) in order to infer the possible ZAMS mass and age of the central star.

3.2. *Individual Objects*

a) A 14 Images of A 14 with the [N II] 6584, Hα, *H2*, and [O III] 5007 filters are presented in Figure 1. The exquisite bipolar shape of A 14 seen in [N II] 6584 is not replicated in any of the other images: the object is a diffuse elliptical nebula in Hα, diffuse and more concentrated in [O III] 5007, and there is no hint of molecular hydrogen emission within it. Not surprisingly, there is a limited amount of spectral information in this intrinsically faint PN (see Tables 2a and 5), and a larger than usual solid angle was inspected: the slit was aligned in the NS direction, and the spectrum is the sum of two extractions centered 11.5″ N and S of the PNN, with each aperture 11.5″ long. The distinguishing properties of the spectrum are the high intensity of the N^+ lines, implying a large nitrogen abundance, and the absence of any O^+ or O^0 line, which indicates that the nebula is optically thin. It should also be noticed that there may be shock excitation in the region since Hα/[S II] 6724 is rather low (Table 5). The chemical abundances reported in Table 4a are gross estimates since, in the absence of detectable emission from [O III] 4363 and information on any O^+ line, assumptions were made on $T(O^{+2})$ (see Table 4a) and the oxygen abundance. From the spectrum it can be estimated that the flux of [O II] 3727 is less than about 2×10^{-14}, which implies that $O^+/H^+ \leq 6\times10^{-5}$ and $O/H \leq 1.3\times10^{-4}$ (these numbers are two times larger for [O II] 7320). These upper limits were assumed when determining the other abundances reported in Table 4a, which are clearly those of a type I PN. The nitrogen and sulfur abundances are larger than the numbers

TABLE 4

ABUNDANCES

Ion	Line	A 14[a]	A 24[a]	A 79	DeHt 3	K 3-46	K 3-91[a]	KjPn 6[c]
He^{+}	5876	0.119	0.254	0.199	0.109	0.170	0.099	0.113
He^{+2}	4686	0.037	0.028	0.045	0.030	0.024	0.087	...
O^{0} $\times 10^{-5}$	6300	...	...	7.26	3.97	4.39	3.08	...
O^{+} $\times 10^{-4}$	3727	...	1.30	1.32	1.86	1.04	...	...
O^{+} $\times 10^{-4}$	7325	...	...	2.51	...	1.35	0.51	...
O^{+2} $\times 10^{-4}$	5007	0.48	0.51	0.43	1.78	0.69	2.31	0.51
N^{0} $\times 10^{-5}$	5200	0.91	1.50	1.55	0.15	1.14	...	0.20
N^{+} $\times 10^{-5}$	6584	18.0	37.2	31.3	4.23	27.5	6.79	12.0
S^{+} $\times 10^{-6}$	6717	1.33	2.55	4.65	1.00	3.15	0.31	0.51
S^{+2} $\times 10^{-6}$	6312	...	...	...	...	...	...	...
Ne^{+2} $\times 10^{-5}$	3869	...	8.96	3.88	5.96	6.07	...	...
Ne^{+3} $\times 10^{-5}$	4725	...	...	...	...	...	...	...
Ar^{+2} $\times 10^{-6}$	7136	1.14	2.59	1.79	...	2.20	1.12	...
Ar^{+3} $\times 10^{-7}$	4740	...	...	...	2.44	...	...	...
Ar^{+4} $\times 10^{-7}$	6435,7006	...	...	...	...	...	...	...
Cl^{+2} $\times 10^{-7}$	5528	...	...	...	...	...	...	...
Element		A 14[b]	A 24	A 79	DeHt 3	K 3-46	K 3-91	KjPn 6[c]
He	...	0.156	0.282	0.244	0.139	0.194	0.186	0.113
O $\times 10^{-4}$	...	1.30	1.93	2.00	4.28	1.89	4.29	1.78
N $\times 10^{-4}$	...	3.90	5.52	4.74	0.97	5.00	5.71	1.68
S $\times 10^{-6}$	...	9.30	16.4	29.6	7.11	21.2	3.46	3.27
Ne $\times 10^{-5}$	...	...	33.9	18.1	14.3	16.6	...	...
Ar $\times 10^{-6}$	...	2.10	4.84	3.34	...	4.11	2.09	...

[a] A 14, A 24, K 3-91 and KjPn 6 ionic abundances assuming that $T(O^{+2}) = T(N^{+}) + 1000$.

[b] A 14 abundances determined assuming that the oxygen abundance is 1.30×10^{-4}.

[c] KjPn 6 abundances determined assuming that the oxygen abundance is 1.78×10^{-4}.

given in Table 4a if the oxygen abundance is smaller. The oxygen, nitrogen and sulfur abundances calculated with the oxygen temperature derived from the $T(O^{+2})/T(N^{+})$ vs. He II 4686 relation given by KB (15,400 K) are $\sim$ 10% smaller than the values given in Table 4a.

The Zanstra temperature (151,000 K, Table 5) and PNN evolutionary tracks (VW 94 and BL 95) imply that A 14 cannot be younger than a few thousand years for any ZAMS precursor. But since the nebula is probably optically thin, the central star effective temperature must be lower. If so, the precursor mass could not have been larger than 3 $M_{\odot}$ when in main sequence. The evolutionary tracks for the 3.0 $M_{\odot}$ model from BL95 and the 2.5 $M_{\odot}$ model of VW94 lead to similar conclusions regarding the properties of the PNN: $\sim 200\,L_{\odot}$ and an age close to 8000 yr. The destruction of the molecular material by the photodissociation front and the overall optical appearence of A 14 are consistent with this age estimate.

b) A 24 The large strength of the He^{+} and N^{+} lines lead to substantial helium and nitrogen abundances (Table 4a), and clearly imply that A 24 is a low-excitation (weak [O III] 5007 emission, Table 2a) type I PN. The oxygen temperature could not be measured, and it was assumed to be 1000 K larger than the temperature derived from the nitrogen lines. The concentration of He^{+} is very large, regardless of the assumed oxygen temperature (0.245 if $T(O^{+2}) = 8000$ K and 0.284 if $T(O^{+2}) = 11,400$ K, as deduced from the $T(O^{+2})/T(N^{+})$ vs. He II 4686

TABLE 4 (CONTINUED)

Ion	Line	M 1-28	M 1-57	M 3-3	M 3-5	NGC 2818	Sh 1-89	Wray 16-22
He^{+}	5876	0.097	0.073	0.118	0.094	0.121	0.134	0.079
He^{+2}	4686	0.042	0.058	0.018	0.041	0.036	0.030	0.012
$O^{0}\ \times 10^{-5}$	6300	2.64	1.89	4.82	1.51	6.22	14.3	0.98
$O^{+}\ \times 10^{-4}$	3727	0.83	0.39	1.25	0.37	1.30	2.86	0.44
$O^{+}\ \times 10^{-4}$	7325	0.84	...	1.44	0.57	2.87	1.59	...
$O^{+2}\ \times 10^{-4}$	5007	0.86	2.40	1.91	1.56	0.91	2.45	1.39
$N^{0}\ \times 10^{-5}$	5200	1.31	0.19	1.50	0.18	0.94	1.52	...
$N^{+}\ \times 10^{-5}$	6584	22.9	3.51	25.6	4.33	17.6	21.4	0.94
$S^{+}\ \times 10^{-6}$	6717	2.72	1.24	0.36	0.26	3.45	2.64	0.67
$S^{+2}\ \times 10^{-6}$	6312	8.21	5.44	...	0.86	3.03	...	2.02
$Ne^{+2}\ \times 10^{-5}$	3869	4.14	5.50	5.02	3.96	4.61	12.9	3.86
$Ne^{+3}\ \times 10^{-5}$	4725	...	14.7	...	...	...	...	...
$Ar^{+2}\ \times 10^{-6}$	7136	2.19	...	1.53	1.07	1.80	1.64	...
$Ar^{+3}\ \times 10^{-7}$	4740	3.57	8.02	...	2.27	...	...	...
$Ar^{+4}\ \times 10^{-7}$	6435,7006	...	3.96	...	0.36	...	...	...
$Cl^{+2}\ \times 10^{-7}$	5528	1.62	0.66	...	0.40	...	...	...
Element		M 1-28	M 1-57	M 3-3	M 3-5	NGC 2818	Sh 1-89	Wray 16-22
He		0.139	0.131	0.136	0.135	0.157	0.163	0.091
O $\times 10^{-4}$		2.15	4.12	3.47	2.46	2.63	6.07	2.00
N $\times 10^{-4}$		5.92	3.74	7.11	2.91	3.56	4.54	0.43
S $\times 10^{-6}$		11.9	10.5	2.76	1.55	6.79	18.4	6.08
Ne $\times 10^{-5}$		10.4	20.2	9.12	6.23	13.4	32.0	5.55
Ar $\times 10^{-6}$		4.15	1.32	2.86	1.57	3.37	3.07	...

relation given by KB) or the the He I line used ($He^+/H^+ = 0.251$ and 0.257 from He I 4471 and 6678 Å). Regardless of the assumed oxygen temperature, the occurence of third dredge-up episodes in the progenitor is implied by the chemical composition of the PN, in particular by its large neon abundance. The intensity of the S^+ lines at 6724 Å relative to Hα suggests that the ionized component may be subject to shock excitation. The absence of detectable [O I] 6300 emission (Table 2a) indicates that A 24 is optically thin, so that the central star temperature must be less than the Zanstra temperature given in Table 5 (131,000 K). If so, the theoretical evolutionary tracks for central stars imply that the ZAMS mass of the progenitor was not larger than about 3 $M_\odot$ (VW94 and BL95).

Excellent images of of A 24 in the light of [O III] 5007, Hα, and [N II] 6584 were produced by Hua & Kwok (1999). For the sake of completeness a [N II] 6584 image of A 24 is shown in Figure 2, where the position of the slit is indicated. The object is too faint and/or diffuse in other optical emission lines (particularly in [O III] 5007). Molecular hydrogen emission could not be found some 200″ around the position where the spectrum was taken. The low central star temperature (for a type I PN), the extension and low density of the nebula and the absence of detectable molecular hydrogen emission indicate that A 24 is an evolved PN. For obvious reasons it was classified as elliptical in the IAC-Catalog. Since its chemical makeup has the unmistakeable signature of a type I PN it is not unlikely that it is a bipolar seen nearly pole-on. If so, as noticed by Hua & Kwok (1999), the bright lobes of enhanced emissivity can be interpreted as traces of a disrupted torus in an evolved nebula. It should also be noticed that the total Hα flux reported by Hua & Kwok (1999) is 2.5 times smaller than the number given in Table 5. This may related to the different way in which the Hα images were flux-calibrated.

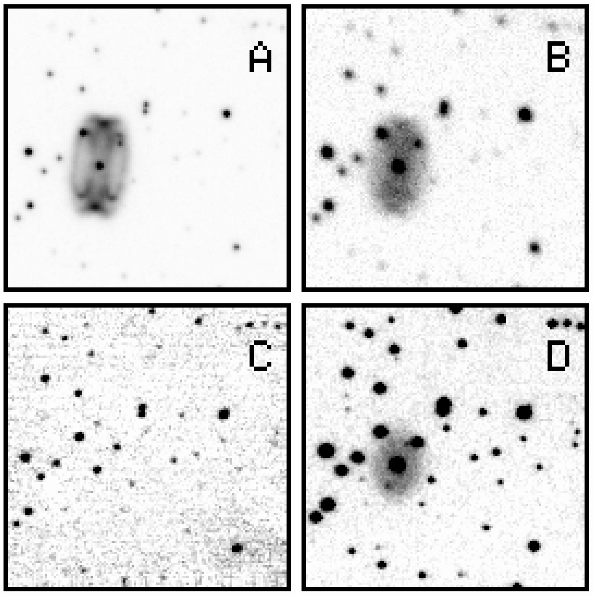

Fig. 1. A 14 in (*a*) [N II] 6584, (b) Hα, (c) *H2* and (d) [O III] 5007. The field-of-view (FOV) is $110'' \times 110''$. North is up, east is to the left.

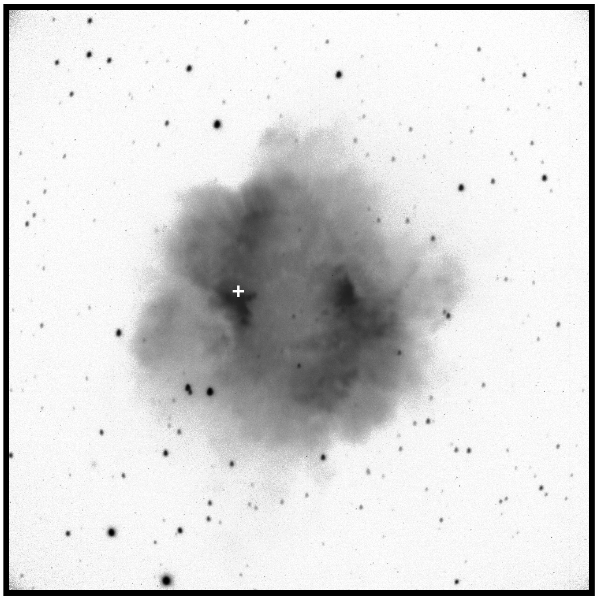

Fig. 2. A 24 seen in [N II] 6584 (logarithmic scale). The position where the spectrum was taken is marked by a cross. The FOV is $717'' \times 717''$, north is up and east is to the left.

Large and structured variations in the [N II] 6584/Hα line ratio—which can be as high as 7 and as low as 1—within the central region of A 24 can be seen in the corresponding image displayed in Figure 3. It is extremely unlikely that this is due to variations in the nitrogen-to-hydrogen abundance ratio. Thus, the image depicts large changes in the concentration of singly ionized nitrogen (N^+/H^+) and/or smaller ones in the electron temperature. Some $60''$ away from the central star there is a marked increase in [N II] 6584/Hα, which can be accounted for if the electron temperature is larger by up to 20% (an overestimate, since N^+/H^+ could also be larger). An additional and striking pattern is the existence of extended radial "filaments". Locally, these structures can be explained with changes not larger than 10% in the electron temperature. It is probably true that the behaviour of the [N II] 6584/Hα line ratio is mainly due to temperature variations in the nebula. The interpretation of these variations (and their origin) depends fundamentally on the real morphology of A 24. These are obviously radial if the nebula is elliptical, but if it is a bipolar seen pole-on these occur ("slide") over the inner surface of the cone.

c) A 79 A 79 is a PN with what may be the smallest Hα/[S II] 6724 line ratio reported in a PN (Tables 2a and 5). Rodríguez, Corradi, & Mampaso (2001) also found this ratio to be very small, and in an Hα/[S II] 6724 image (not shown) it can be seen that it is almost always smaller than ~ 2 in the brightest regions of the PN. The strength of the S^+ lines suggests that the gas is also being excited by shock waves, a suspicion that is supported by the large temperature difference between the N^+ and O^{+2} regions ($T(O^{+2})/T(N^+) = 1.41$, see Tables 3 and 5). Thus, the reported abundances (Table 4a) may be suspect due to the likely existence of shock excitation in the ionized component. Even so, the large helium and nitrogen-to-oxygen abundances are unquestionable and indicative of a highly enriched type I PN. The large abundance of neon and high N/O ratio imply third dredge-up episodes during the thermally pulsating AGB phase. An additional interesting property in the spectrum of A 79 is the great strength of the [N I] 5200 and [O I] 6300 lines (see Table 2a), which imply that the observed region is optically thick and that maybe up to 15–30% of the material is neutral (see the ion abundances, Table 4a). The central star Zanstra temperature of this optically thick PN is 180,000 K (Table 5), but notice that the He II 4686 Å intensity reported by Rodríguez et al. (2001) leads to much higher (and not too plausible) temperatures. In the context of VW94 models this temperature implies a PNN age and luminosity between 2500 and 3500 yr and 1000 and 200 $L_\odot$ for a ZAMS progenitor mass between 2.5 and 5.0 $M_\odot$. Following BL95, the im-

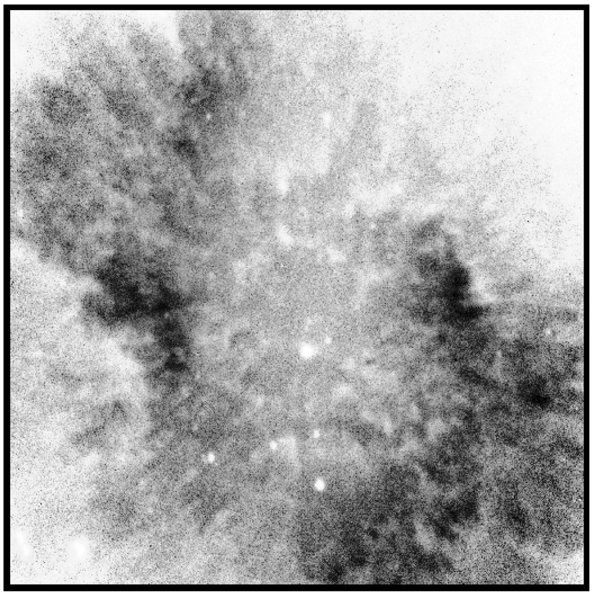

Fig. 3. [N II] 6584/Hα image of A 24. The FOV is $256'' \times 256''$, north is up and east is to the left.

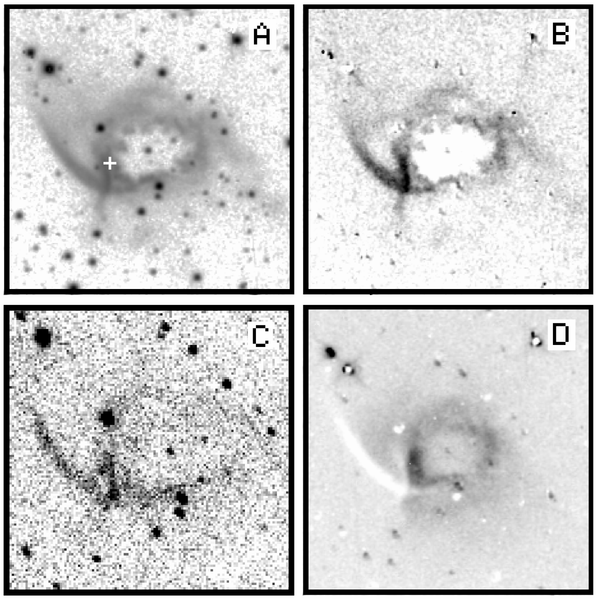

Fig. 4. A 79 in (*a*) [N II] 6584, (*b*) [N II] 6584/Hα, (*c*) *H2*, and (*d*) [O III] 5007/Hα (not corrected for reddening). The position where the spectrum was taken is marked by a cross in (*a*). The FOV is $150'' \times 150''$ in the optical frames and $110'' \times 110''$ in the H_2 image. North is up, east is to the left.

plied age and luminosity are 900 yr and 500 $L_\odot$ for a 4.0 $M_\odot$ ZAMS progenitor, or 10,000 yr and 300 $L_\odot$ for a 5.0 $M_\odot$ ZAMS progenitor.

Images of A 79 are shown in Figure 4: (*a*) [N II] 6584 (logarithmic scale), (*b*) [N II] 6584/Hα, (*c*) *H2*, and (*d*) [O III] 5007/Hα (not corrected for reddening). Recently published (Hua & Martinis 2002) images of the region showed the presence of extended faint Hα emission in the field as well as the full extension of the southern lobe of A 79 in [N II] 6584. The nebula is invisible in the image taken with the *cK* filter, which confirms the existence (first shown in the excellent images of KWGMP) of shocked molecular hydrogen in this PN. As in many other objects, the distribution of shocked H_2 and [N II] 6584 is very similar. A comparison between the [N II] 6584/Hα and [O III] 5007/Hα images reveals a clear separation between the low and high excitation plasma, the latter being usually closer to the central exciting star, where [O III] 5007/Hα can be as high as $\sim$ 3.5 (corrected for reddening). This segregation is particularly obvious in the lowly excited eastern filament, where [N II] 6584/Hα $\sim$ 6.8–7.5 and [O III] 5007/Hα $\sim$ 0.1-0.5.

d) DeHt 3 The oxygen and neon abundances (Table 4a), as well as the nitrogen-to-oxygen abundance ratio (Table 5), of this highly excited optically thin object are characteristic of type II PNe, where the ZAMS progenitor mass is expected to be around 1.5 $M_\odot$ (Peimbert 1990). The helium abundance (0.139 from He I 5876 Å, 0.129 from He I 6678 Å) is significantly larger than the mean value found in these objects (0.11). This abundance setup (low N/O ratio and large He abundance) has been found in a few other PNe (e.g., KB and BJ). Images of DeHt 3 in Hα, Hβ, [O III] 5007, [N II] 6584, *H2*, and *cK* were obtained. Since the object morphology is very similar in all optical emission lines, only the [N II] 6584 image is shown in Figure 5, where it can be seen that DeHt 3 is an asymmetrical elliptical PN with no additional features, such as ansae, jets or point symmetric structures. Optical line ratios (i.e., excitation conditions) are quite uniform throughout it, and the only significant (and expected) difference is that the intensity peaks of [N II] 6584 and [O III] 5007 are separated some 3″, the latter being closer to the geometrical center. In the *H2* image (not shown) there is very faint emission in the region occupied by the PN. This is not seen in the *cK* image. If this is confirmed, the persistence of molecular hydrogen in this type II PN would imply that DeHt 3 is a relatively young object. This would not be surprising given the highly excited nature of its spectrum and the large Zanstra temperature (137,000 K, an upper limit to the real effective temperature since the inspected region is optically thin).

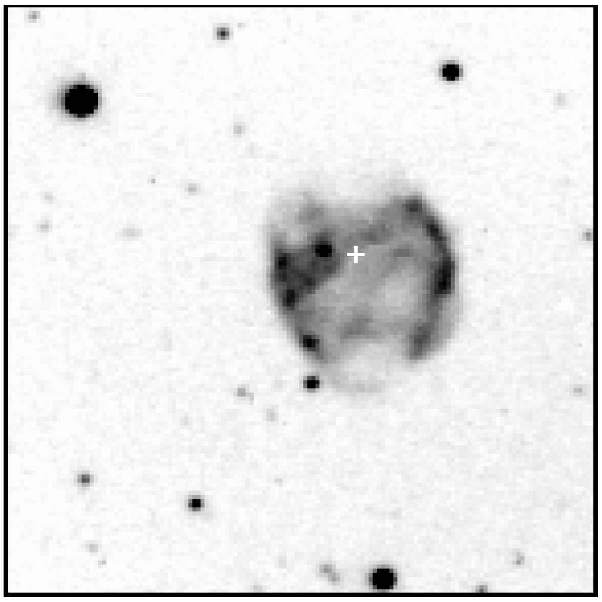

Fig. 5. [N II] 6584 image of DeHt 3 (logarithmic scale). The FOV is $90'' \times 90''$. North is up, east is to the left.

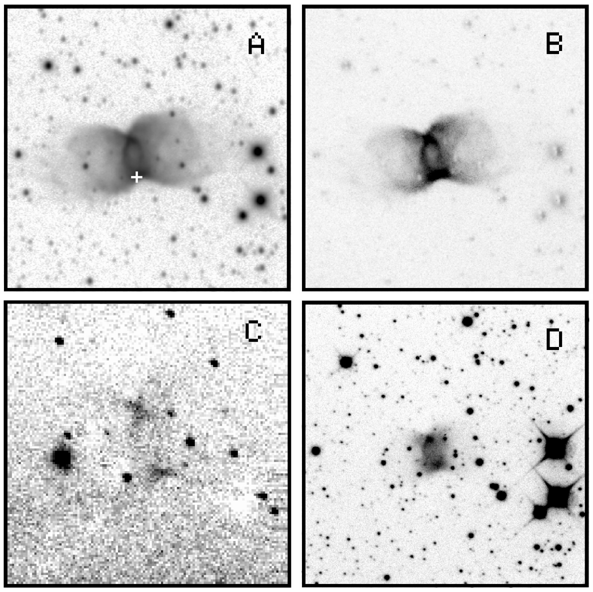

Fig. 6. K 3-46 in (*a*) [N II] 6584 (logarithmic scale), (*b*) [N II] 6584/Hα, (*c*) *H2*, and (*d*) [O III] 5007. The position where the spectrum was taken is marked by a cross in *a*. The FOV in frames *a*, *b*, and *d* is $190'' \times 190''$, and $110'' \times 110''$ in frame *c*. North is up, east is to the left.

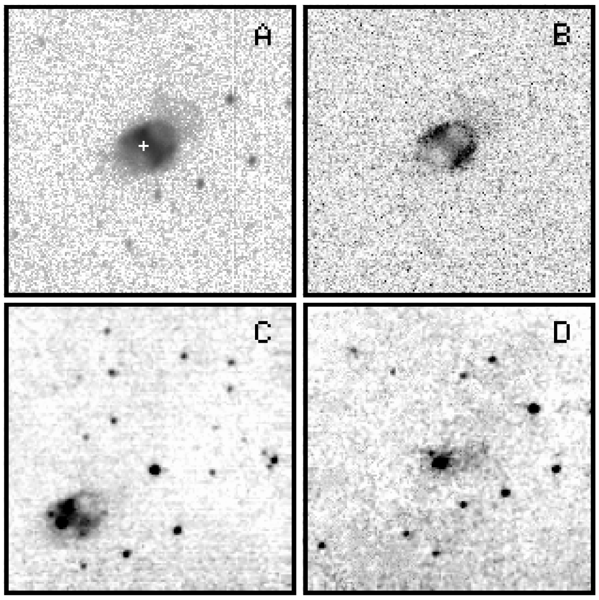

Fig. 7. K 3-91 in (*a*) [N II] 6584 (logarithmic scale), (*b*) [O III] 5007, (*c*) *H2*, and (*d*) *cK*. The position where the spectrum was taken is marked by a cross in *a*. The FOV is $110'' \times 110''$. North is up, east is to the left.

e) K 3-46 The spectrum (Table 2a) of this mildly excited optically thick object is characterized by the similar relative intensities of lines from low and high ionization species. The Hα/[S II] 6724 ratio (1.66) indicates that shock excitation is significant in the ionized component. The electron temperature in the O^{+2} region was not determined, and the temperature ratio could not be used to support this possibility. The chemical composition reported in Table 4a is for $T(O^{+2}) = T(N^{+}) + 1000$ K, but since the sulfur lines are very intense it is likely that $T(O^{+2})$ is even larger (BJ). Abundances are typical of a type I PN, a foregone conclusion given the large intensity of the helium and nitrogen lines. For $T(O^{+2}) = 13,300$ K, the value derived from the $T(O^{+2})/T(N^{+})$ vs. He II 4686 relation given by KB, it is found that He = 0.194, O = 1.68×10^{-4}, N = 4.44×10^{-4}, S = 2.06×10^{-5}, Ne = 1.40×10^{-4}, and Ar = 4.11×10^{-6}. Bear in mind that these abundances are suspect given the possible presence of shocks in the plasma.

Images of K 3-46 are shown in Figure 6: (*a*) [N II] 6584 (logarithmic scale), (*b*) [N II] 6584/Hα, (*c*) *H2*, and (*d*) [O III] 5007. The nearly perfect bipolar morphology, the close correlation between the regions of enhanced H_2 and [N II] 6584 emissivity, the limited extent of the the [O III] 5007 emission region and the presence of shocked H_2 (first shown by KWGMP) are all typical of a well developed middle-aged type I PN. The Zanstra temperature of the central star is

125,000 K. The hydrogen-burning models of VW94 and BL95 for ZAMS progenitors more massive than $3.5\,M_\odot$ achieve this temperature either too early (before 1000 yr) or too late (after 30,000 yr). The evolutionary track of the $3.0\,M_\odot$ ZAMS progenitor model from BL95 implies an age of 6000 yr ($L = 4000\,L_\odot$) or 8400 yr ($L = 2800\,L_\odot$). In the VW94 H-burning model for the $2.5\,M_\odot$ ZAMS progenitor there is a wider range: 1800 ($L = 14,000\,L_\odot$) or 14,000 yr ($L = 125\,L_\odot$).

f) K 3-91 As evinced by the intensity of [O III] 5007 (Table 2b), K 3-91 is one of the most highly excited objects in the sample. Information on important emission lines at the blue end of the spectrum ([O II] 3727, [Ne III] 3869, and [O III] 4363) could not be obtained since extinction is quite high. Of particular interest is the strength of He II 4686, which leads to very large values for the He^{+2}/He^{+} ratio (0.88) and the Zanstra temperature (250,000 K, see Table 5). The latter is an overestimate since the weakness of the O^0 lines (which lead to a very small fraction of neutral material, less than $\sim 5\%$) and the non-detection of [N I] 5200 imply that K 3-91 is optically thin. Shock excitation can be discarded since the sulfur lines are very weak when compared to Hα. Abundances (Table 4a) were calculated assuming that $T(O^{+2}) = T(N^{+}) + 1000$ K. These indicate that K 3-91 is a type I PN. From the intensity of He II 4686, the relation provided by KB yields $T(O^{+2})/T(N^{+}) = 1.44$. Abundances resulting from the oxygen temperature derived from this relation (17,100 K) are as follows: He = 0.185, $O = 2.47 \times 10^{-4}$, $N = 3.29 \times 10^{-4}$, $S = 2.76 \times 10^{-6}$, and $Ar = 2.09 \times 10^{-6}$. But these abundances are suspect since this high temperature ratio is usually found in objects where Hα/[S II] 6724 is also small (BJ), which is clearly not the case in K 3-91 (Table 5).

The Zanstra temperature, though clearly larger than the effective temperature of the central star, does suggest that the latter is quite high and, in consequence, that K 3-91 is being illuminated by a relatively massive and possibly young PNN, the end product of the evolution of a star with a ZAMS mass larger than $\sim 3.5\,M_\odot$ (VW94 and BL95).

Images of K 3-91 are shown in Figure 7: (*a*) [N II] 6584 (logarithmic scale), (*b*) [N II] 6584/Hα, (*c*) *H2*, and (*d*) *cK*. There is no clear evidence of a well developed bipolar morphology, though the faint "fan" extending to the NW (seen in the [N II] 6584 image) may be an incipient lobe. If it is so, K 3-91 is indeed a young PN, as the spectrum and the Zanstra temperature combined with evolutionary models seem to imply. As in other bipolar PNe, [N II] 6584/Hα is larger in the central torus than in the arcs around it (e.g., K 3-72, BJ), and the emission of [O III] 5007 is concentrated in the central part (this image is not shown). The presence of molecular gas is quite clear. This is in stark contrast with the apparent absence of neutral material (at least in the region covered by the spectral slit), and can only mean that the photodissociation front is followed very closely by the photoionization front. A comparison between the *H2* and *cK* images indicates that most of the infrared emission seen in the *H2* frame is probably due to shock excited H_2, again a typical feature of type I PN. An inspection of the *H2*/*cK* image ratio (matching the background and then the star counts) yields values of $\sim$ 3–4 in the area where extended emission is seen in the *cK* frame (to the west), which implies that infrared emission in this region is due to dust or photoexcitation.

g) KjPn 6 From its spectrum and nitrogen temperature (Tables 2b and 3) it can be established that KjPn 6 is a low excitation optically thin object with no shock excitation (Hα/[S II] 6724 = 26.6). Since [O III] 4363 is absent, it was assumed that $T(O^{+2}) = T(N^{+}) + 1000$. The non-detection of [O II] 3727 implies that $O^{+}/H^{+} < 1.27 \times 10^{-4}$, and this number was assumed when abundances were calculated. The resulting chemical composition (Table 4a) is unexpected, regardless of the value assumed for the oxygen temperature. The reported He^{+} abundance (0.113) may be excessive since the other He I lines yield smaller values: 0.079 from He I 4471 and 0.088 from He I 6678. On the other hand $He^{+2}/H^{+} < 0.003$ since He II 4686 Å is also absent in the spectrum. Hence, the relative abundance of ionized helium does not exceed 0.116, less than the limit defining type I PNe. Notice too that the sum of the oxygen and nitrogen abundances ($< 3.46 \times 10^{-4}$) is characteristic of type III PNe (Peimbert 1990). This is not unexpected since the object is at least ~ 800 pc above the galactic plane (Zhang 1995). In contrast to these results, the nitrogen-to-oxygen abundance ratio in KjPn 6 (0.94) is unquestionably that of a type I PN. If there is a substantial amount of neutral helium, which is not unlikely in this low excitation PN, the two defining attributes of a type I PN would be fulfilled. In order to be so, a second dredge-up episode enhancing He and N at the expense of C and O should have occured in the progenitor star in the early AGB stage. To do so, the star must have been more massive than $\sim 3\,M_\odot$ when on the main

TABLE 5

GENERAL PROPERTIES

Object	Type	Mor.	He	N/O	N+O	HeR[a]	TR[b]	HS[c]	$-F_{\alpha}$[d]	$M(\mathrm{H}^{+})$[e]	T_{c}[f]	V_{o}[g]
A 14	I	B	0.156	3.00	5.01	0.31	···	2.80	12.27	$0.8^{+0.8}_{-0.4}$	<151	22.9±0.3
A 24	I	B	0.282	2.86	7.45	0.11	···	3.08	10.47	$12^{+4.1}_{-3.3}$	<131	17.8±0.1
A 79	I	B	0.244	2.37	6.74	0.23	1.41	1.11	11.16	$4.2^{+2.1}_{-1.5}$	180	20.3±0.2
DeHt3	II	E	0.139	0.23	5.25	0.28	1.08	5.34	11.82	$0.5^{+0.2}_{-0.1}$	<137	21.2±0.1
K 3-46	I	B	0.194	2.65	6.89	0.14	···	1.66	11.64	$3.7^{+4.1}_{-2.0}$	125	21.0±0.3
K 3-91	I	B	0.186	1.33	10.0	0.88	···	15.5	11.63	23^{+63}_{-17}	<250	23.0±0.4
KjPn 6	I	B	0.113	1.38	3.40	···	···	24.4	11.84	$3.0^{+4.5}_{-1.8}$	< 85	20.5±0.3
M 1-28	I	B	0.139	2.75	8.07	0.43	1.31	2.35	11.13	$15^{+20}_{-8.6}$	160	20.4±0.3
M 1-57	I	B	0.131	0.91	7.86	0.79	1.01	4.83	11.21	43^{+93}_{-30}	<189	21.2±0.4
M 3-3	I	B	0.136	2.05	10.6	0.15	1.13	18.9	11.84	$1.9^{+1.9}_{-0.9}$	>114	21.2±0.3
M 3-5	I	B	0.135	1.18	5.37	0.44	1.06	17.2	11.54	$3.2^{+2.5}_{-1.4}$	<158	21.1±0.2
NGC 2818	I	B	0.157	1.35	6.19	0.30	1.34	1.48	10.63	$11^{+4.0}_{-3.1}$	149	18.5±0.1
Sh 1-89	I	B	0.163	0.75	10.6	0.22	1.13	3.44	10.72	24^{+26}_{-12}	135	18.8±0.3
Wray 16-22	III	E	0.091	0.21	2.43	0.15	0.97	5.63	11.20	$6.1^{+4.2}_{-2.6}$	103	19.1±0.2

[a]HeR = $\mathrm{He}^{+2}/\mathrm{He}^{+}$. [b]TR = $T(\mathrm{O}^{+2})/T(\mathrm{N}^{+})$. [c]HS = H$\alpha$/[S II]6724. [d]$F_{\alpha}$ = logarithm of the total Hα flux (not de-reddened).

[e]$M(\mathrm{H}^{+})$ = mass of ionized hydrogen in solar mass units, for a distance of 1 kpc and $\langle N_{\mathrm{e}}\rangle = 1\,\mathrm{cm}^{-3}$.

[f]T_{c} = central star temperature in 1000 K. [g]V_{o} = visual magnitude of the central star.

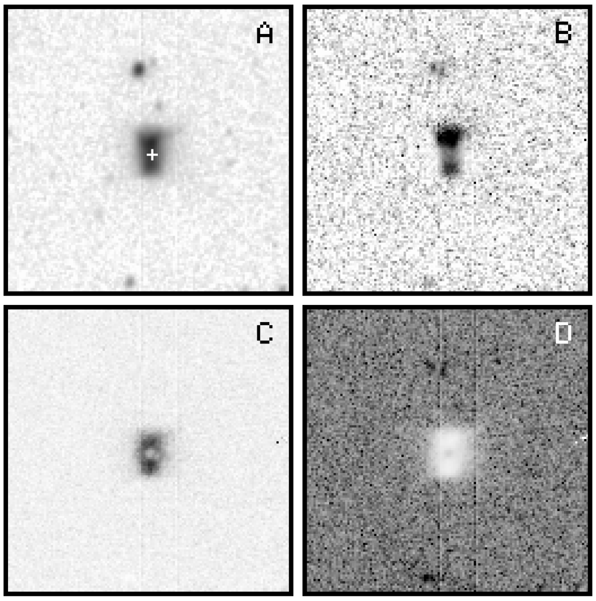

Fig. 8. KjPn 6 in (*a*) [N II] 6584 (logarithmic scale), (*b*) [N II] 6584/Hα, (*c*) Hα/Hβ, and (*d*) [O III] 5007/Hα. The position where the spectrum was taken is marked by a cross in (*a*). The FOV is $90'' \times 90''$. North is up, east is to the left.

sequence (Iben 1995). This is hard to accept given the high Galactic latitude of KjPn 6, but star forming regions at high latitudes, although rare, are not unheard of. For instance, the H II and star-forming region Sh 2-128 (misclassified as PN A 77 in Acker et al. 1992) is nearly 500 pc above the plane (Chini & Wink 1984; Bohigas & Tapia 2003). In this context it is worth noticing that the low N and O abundances suggest that the progenitor star was formed from a molecular cloud where abundances were smaller than present day values. If KjPn 6 is a type I PN theoretical evolutionary tracks indicate that it can not be older than 1000 yr (VW94 2.5 $M_\odot$ model) or 4500 yr (BL95 3.0 $M_\odot$ model), since the central star temperature can not be larger than 85,000 K (the nebula is optically thin and He II 4686 is below the detection limit).

Images of KjPn 6 are shown in Figure 8: (*a*) [N II] 6584 (logarithmic scale), (*b*) [N II] 6584/Hα, (*c*) Hα/Hβ, and (*d*) [O III] 5007/Hα. The optical source seems to be little more than a conspicuous narrow bar extending along the NS axis. A closer inspection reveals that this bar is in fact a tilted disk with faint short filaments emerging from its outer edges, i.e., KjPn 6 is bipolar, like most type I PNe. This is specially evident in the Hα/Hβ image. Notice too that this ratio (extinction) is higher in the disk than elsewhere, a standard signature of type I PNe. On the other hand molecular hydrogen is nearly or totally absent since the nebula was not detected when seen through the *H2* and *cK* filters. In conjunction with the low-excitation spectrum, these images suggest that KjPn 6 is either old and/or was produced by a not too massive progenitor. To finalize, the evidence at hand is marginally favorable towards classifying KjPn 6 as a type I PN, but further research around this object is undoubtedly necessary and will probably provide valuable insights.

h) M 1-28 M 1-28 is a medium excitation PN where nitrogen is obviously overabundant (Table 2b). The Hα/[S II] 6724 ratio (2.35) and the substantial difference in the O^{+2} and N^{+} electron temperatures ($T(O^{+2})/T(N^{+}) = 1.31$) indicate that shock excitation may have some effect on the emission spectrum. Thus, though the chemical composition of M 1-28 is clearly that of a type I PN (Table 4b), the likely presence of shock excitation indicates that abundances are suspect. The Zanstra temperature (160,000 K, Table 5) is possibly larger than the central star temperature since the object is marginally optically thick: line intensities from low ionization species are strong, but the N^0/N and O^0/O ratios (Table 4b) imply that there is not a great amount of neutral gas, though the presence of molecular material is clear.

Images of M 1-28 are displayed in Figure 9: (*a*) [N II] 6584 (logarithmic scale), (*b*) [N II] 6584/Hα, (*c*) *H2*, and (*d*) [O III] 5007. As shown by KWGMP, molecular hydrogen emission is due to shock excitation, and its distribution follows closely the regions where [N II] 6584 is more intense (where [N II] 6584/Hα is larger). As in other bipolar type I PNe, most of the optical emission is concentrated in the central torus. The highly excited gas is clearly more confined: the length of the "waist" of the bipolar nebula is about $23''$ when seen in [O III] 5007, $27''$ in the light of [N II] 6584, and $29''$ in H_2. These images suggest that M 1-28 is a middle aged PN, since the structure is well developed and H_2 emission is conspicuous. If so, theoretical evolutionary tracks and the Zanstra temperature imply that the ZAMS progenitor mass was around 3.0 $M_\odot$, and that the PNN age and luminosity are between $\sim$ 3000–7000 yr and 250–2000 $L_\odot$ (VW94 and BL95).

i) M 1-57 M 1-57 is a bright and probably young PN. Some clearly identified emission lines that are not reported in Table 2b, are the following (line intensity corrected for reddening in parenthesis, with Hβ = 100): [S II] 4069 (17.3), [S II] 4076

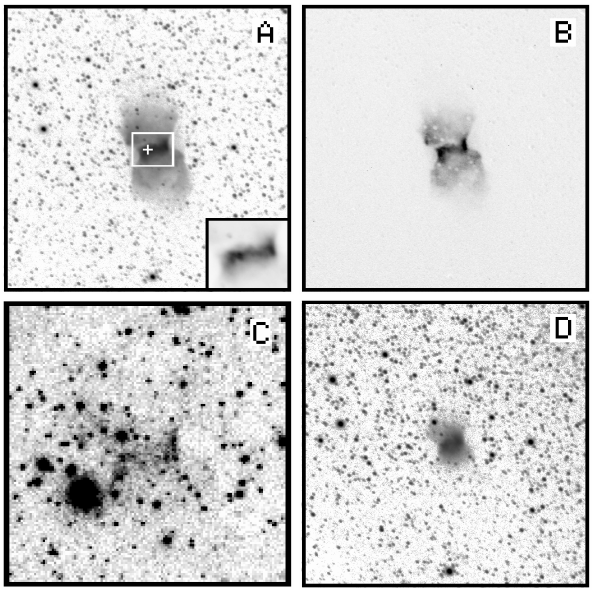

Fig. 9. M 1-28 in (*a*) [N II] 6584 (logarithmic scale), (*b*) [N II] 6584/Hα, (*c*) *H2*, and (*d*) [O III] 5007. The central region of the [N II] 6584 image is displayed in the *a* subframe. The position where the spectrum was taken is marked by a cross in *a*. The FOV is $256'' \times 256''$ in frames *a*, *b* and *d*, $110'' \times 110''$ in frame *c* and $35'' \times 30''$ (EW and NS) in the *a* sub-frame. North is up, east is to the left.

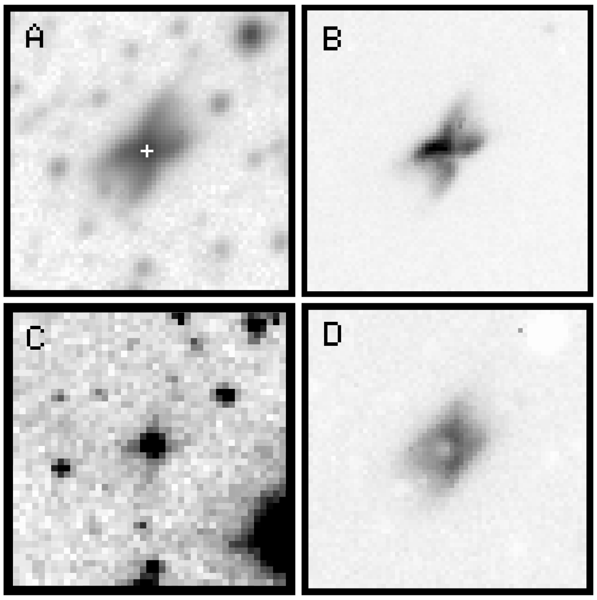

Fig. 10. M 1-57 in (*a*) [S II] 6724 (logarithmic scale), (*b*) [N II] 6584/Hα, (*c*) *H2* and (*d*) Hα/Hβ. The position where the spectrum was taken is marked by a cross in frame *a*. The FOV is $40'' \times 40''$. North is up, east is to the left.

(5.21), N III 4634 (1.69), N III 4640 (2.61), [Fe VII] 5159 (0.84), [Fe VI] 5176 (0.80), [Fe VII] 5721 (2.97), [Ca V] and/or [Fe V] 6087 (4.26) and [K IV] 6102 (0.58). Perhaps the most salient property of the spectum of M 1-57 is the high degree of excitation that is manifest in various emission lines from highly ionized species, such as Fe^{+5} and Fe^{+6}, as well as a large He^{+2}/He^{+} ratio (0.79) and the vast amount of Ne^{+3} (nearly 75% of all neon, Table 4b). The Hα/[S II] 6724 and $T(O^{+2})/T(N^{+})$ ratios (4.83 and 1.01, respectively) imply that shock excitation is of no consequence. Both temperatures are large and the electron density is very high, suggesting once more that the object is young. The chemical makeup is of a type I PN (Table 4b) and third dredge-up episodes are suggested by the large neon abundance, though the nitrogen-to-oxygen abundance ratio (0.91) and the helium enrichment in particular (0.131) are not excessive. Milingo, Henry, & Kwitter (2002) determined the chemical composition of this object with a spectrum of a less highly excited region (MKHC). They derive larger oxygen, nitrogen and specially argon abundances, smaller concentrations for neon and sulfur and a nearly identical nitrogen-to-oxygen abundance ratio. The occurence of third dredge-up episodes are not necessarily implied by their neon abundance. It is uncertain if the observed region is optically thick since [O II] 3727 is not particularly intense and the concentration of neutral-to-total nitrogen and oxygen (Table 4b) indicates that there is a small amount of neutral hydrogen, not more than a few percent. Thus, the Zanstra temperature (189,000 K, Table 5) is probably somewhat larger than the effective temperature of the central star. If the real and Zanstra temperatures are similar, evolutionary tracks for ZAMS 2.5–4.0 $M_\odot$ progenitors imply that M 1-57 is a young object, not older than about 3000 yr (VW94 and BL95).

Images of M 1-57 are displayed in Figure 10: (*a*) [S II] 6724 (logarithmic scale), (*b*) [N II] 6584/Hα, (*c*) *H2*, and (*d*) Hα/Hβ. The presence of shock excited H_2 emission can be excluded since the faint extensions emerging from the central star in the *H2* frame are replicated at the same intensity level when the *cK* filter is used. This means that these extensions are probably due to dust in the region. The bipolar structure is well developed, but the central ring confining the outflow is very small. It is worth noting the conspicuous asymmetry in the Hα/Hβ line ratio, which shows that extinction is larger on the NW half of the nebula. This asymmety has been observed at a spectacular level in NGC 6302 (Bohigas 1994). It is almost certainly local, but no explana-

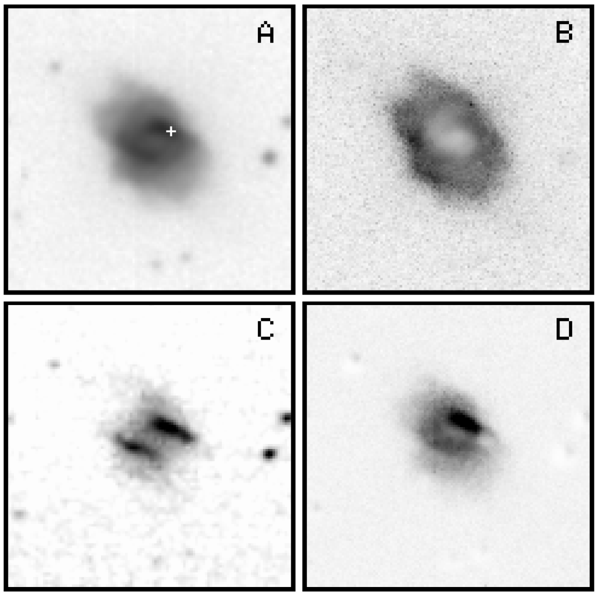

Fig. 11. M 3-3 in (*a*) [N II] 6584 (logarithmic scale), (*b*) [N II] 6584/Hα, (*c*) *H2*, and (*d*) Hα/Hβ. The position where the spectrum was taken is marked by a cross in frame *a*. The FOV is $60'' \times 60''$. North is up, east is to the left.

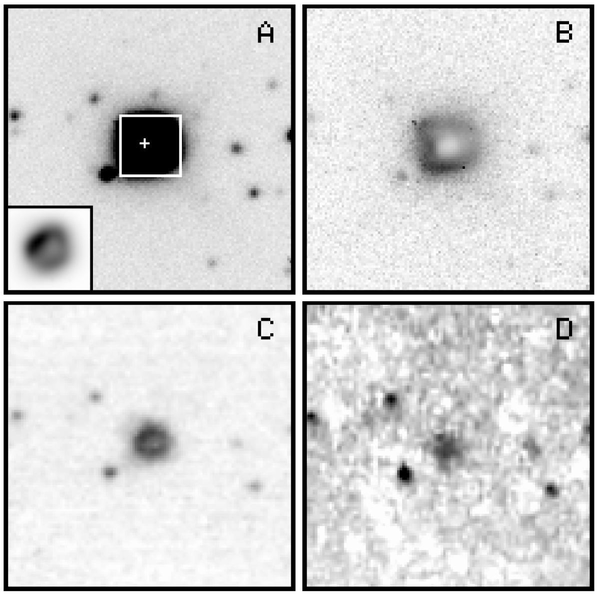

Fig. 12. M 3-5 in (*a*) [N II] 6584, (*b*) [N II] 6584/Hα, (*c*) *H2*, and (*d*) *cK*. The position where the spectrum was taken is marked by a cross in *a*. The FOV is $60'' \times 60''$ in all frames and $12'' \times 12''$ in the *a* sub-frame. North is up, east is to the left.

tion has been put forward. The [N II] 6584/Hα image shows different excitation conditions in the four extensions of the bipole, which are clearly not related to the asymmetric extinction distribution.

j) M 3-3 Spectroscopic observations of this type I PN have been carried out by three groups (PTP, KSK, and KB). A comparison between their spectra and the one presented here (Table 2b) shows that the region observed in this work (with an appreciably smaller aperture) has a significantly larger extinction and is less excited (for instance, compare the intensities of He II 4686 and [S II] 6724). All these spectra show that shock excitation of the ionized gas in M 3-3 is insignificant (in this work Hα/[S II] 6724 = 18.9 and $T(\mathrm{O}^{+2})/T(\mathrm{N}^{+}) = 1.13$). Their data were reanalyzed following the procedure used here, and the resulting abundances (particularly those from PTP) are similar to those reported in Table 4b. These abundances (He = 0.136, N/O = 2.05 and a mild neon enrichment) imply that M 3-3 was produced by a comparatively low mass progenitor of a type I PNe. All spectra are from optically thick regions, and the Zanstra temperature should be close to the central star effective temperature. But since He II 4686 is at least half as bright as previously reported, the Zanstra temperature given in Table 5 (114,000 K) is substantially less than what is derived from the data supplied by PTP, KSK, and KB (all around 150,000 K). This exemplifies the caution that must be exercised when global parameters are derived from localized data. The effective temperature of the PNN is close to 150,000 K after about 2500 yr in the 2.5 $M_\odot$ ZAMS progenitor model produced by VW94, or 7000 yr in the 3.0 $M_\odot$ ZAMS progenitor model developed by BL95.

Images of M 3-3 are displayed in Figure 11: (*a*) [N II] 6584 (logarithmic scale), (*b*) [N II] 6584/Hα, (*c*) *H2*, and (*d*) Hα/Hβ. A bipolar structure with an extended collimating toroid at the center is immediately apparent, and the overall appearence of the nebula suggests it is a middle-aged PN. As in many other bipolar type I PNe, there is abundant shock-excited H_2 emission, predominantly in the toroid. Notice that in this object the toroid has been nearly disrupted. The distribution of [N II] 6584 and H_2 emission is similar, and [O III] 5007 is most intense within the torus (the image is not shown). The central torus is $\sim 8''$ wide in H_2, $7''$ in [N II] 6584 and barely $5''$ in [O III] 5007. Extinction, seen through the Hα/Hβ frame, is quite variable and there is an obvious distinction between the central ring and the remaining nebula. But the most relevant feature of the Hα/Hβ image is the striking difference between the NW ($C(\mathrm{H}\beta) \sim 1.8$) and SE ($C(\mathrm{H}\beta) \sim 0.5$) parts of the torus.

k) M 3-5 Spectroscopic observations of M 3-5 have been conducted by KKSB and KB, who find a nitrogen-to-oxygen abundance ratio that is characteristic of type I PNe (~ 0.7), but a defficient helium abundance for this kind of objects (~ 0.107). On the other hand, the oxygen and nitrogen abundances reported by KKSB are two times larger than the values found by KB (this discrepancy persists when both data sets are analysed with the same formalism). As can be seen from Table 2c, M 3-5 is a bright and highly excited PN, properties that are usually associated with young objects. In accordance with this, the density is also larger than usual (Table 3). Evidence for shock excitation is absent (Hα/[S II] 6724 = 17.2 and $T(\mathrm{O}^{+2})/T(\mathrm{N}^{+}) = 1.06$). The nebula is probably not optically thick, considering the intensity of [O II] 3727 and the scant amount of neutral gas that is deduced from the abundance of neutral-to-total oxygen and nitrogen (which imply that less than 5% of hydrogen is atomic). Thus, the reported Zanstra temperature (158,000 K, Table 5) is probably larger than the effective temperature of the PNN. The helium abundance (0.135) and nitrogen-to-oxygen abundance ratio (1.18) that are found here are larger than the aforementioned results and both are consistent with the standard definition of type I PNe.

Images of M 3-5 in (a) [N II] 6584, (b) [N II] 6584/Hα, (c) *H2*, and (d) *cK* are displayed in Fig. 12. The immediate impression is that this object is an elliptical PN, not the usual bipolar morphology of a type I PN. On the other hand, the existence of a bright central $\sim 4''$ ring in the [N II] 6584 and *H2* images and the lobe seen in the latter (not apparent in any other frame) suggests that M 3-5 is a bipolar seen nearly pole-on. If M 3-5 is an elliptical PN it is not clear whether the *H2* image is produced by shocked molecular hydrogen or by emission from the He I doublet at 2.11 μm, but if it is a bipolar the existence of shock excited H_2 is more likely. The second interpretation is supported by the fact that M 3-5 is a type I PN. Another interesting feature is the central faint diffuse emission apparent in the *cK* frame, which can either produced by dust or radiatively excited H_2. Finally, the Hα/Hβ ratio (the image is not shown) is substantially larger in the western portion of the ring, where $C(\mathrm{H}\beta) \simeq 1.8$, than in the rest of the nebula. Extinction has its lowest value ($C(\mathrm{H}\beta) \simeq 0.5$) at the position of the prominent arc-like feature seen in [N II] 6584 (a sub-frame), proving that it is not a region of enhanced emission.

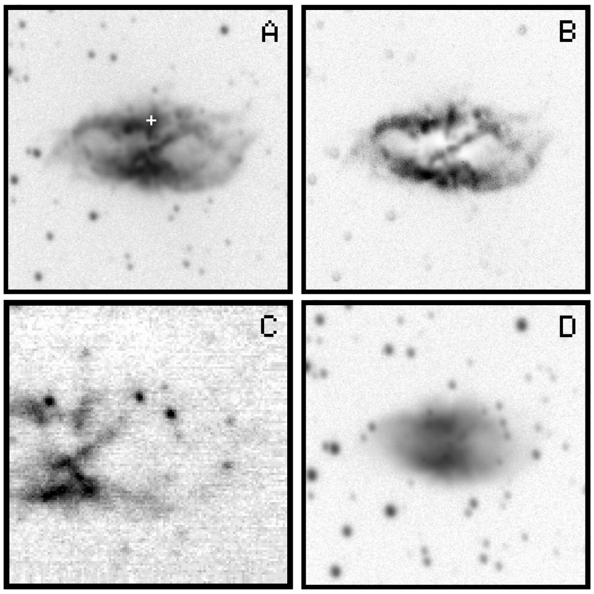

Fig. 13. NGC 2818 in (a) [N II] 6584 (logarithmic scale), (b) [N II] 6584/Hα, (c) *H2*, and (d) [O III] 5007 (logarithmic scale). The position where the spectrum was taken is marked by a cross in a. The FOV is $180'' \times 180''$ in frames (a), (b), and (d), and $110'' \times 110''$ in (c). North is up, east is to the left.

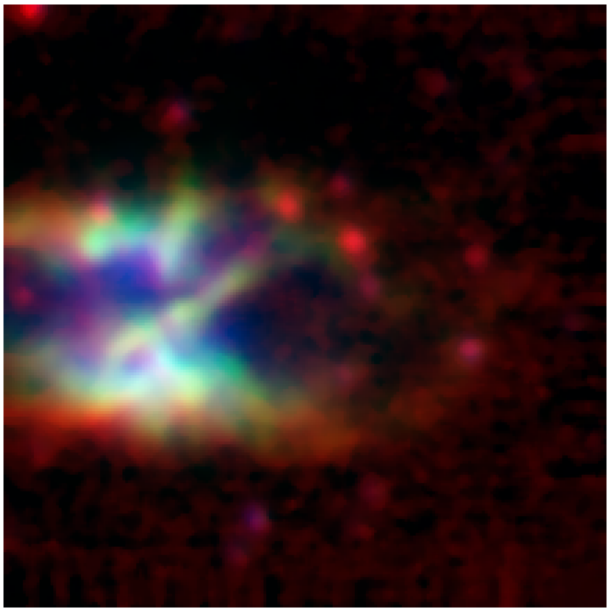

Fig. 14. RGB image of NGC 2818: [O III] 5007 in blue, [N II] 6584 in green and H_2 in red. The FOV is $110'' \times 110''$, north is up and east is to the left.

l) NGC 2818 NGC 2818 was thought to be one of the few PNe in a star cluster (Tifft, Connolly, & Webb 1972). The cluster is at a distance of 2.3 ± 0.2 kpc and is $1.12 \pm 0.12 \times 10^{9}$ yr old, which implies that the mass of a star at the red giant tip is $1.8\,M_\odot$ (Pedreros 1989). This would be the minimum (and approximate) ZAMS mass of the PN progenitor if it is in the cluster. But in a recent paper Mermilliod et al. (2001) found that the radial velocities of the cluster (mean value) and of the PN are very different, and concluded that this association is unlikely. Spectroscopic observations of NGC 2818 have been conducted by DU and PTP in regions with a higher degree of excitation than the one inspected in this work, where He II 4686 and [O III] 5007 are less intense, and $T(\mathrm{O}^{+2})$ and $T(\mathrm{N}^{+})$ (particularly the latter) are smaller (see Tables 2c and 3). Contrary to expectations, the density is 10 times lower in the less highly excited region observed here (only $35\,\mathrm{cm}^{-3}$). Imaging work carried out by Phillips & Cuesta (1998) revealed that there are marked density variations within this object. These authors also noticed that shock excitation may be important in some parts of the nebula. In the observed region $T(\mathrm{O}^{+2})/T(\mathrm{N}^{+}) = 1.34$ and Hα/[S II] 6724 = 1.48, which implies that shock excitation may have a very significant effect on the spectrum. This is not obvious in the regions inspected by DU ($T(\mathrm{O}^{+2})/T(\mathrm{N}^{+}) = 1.20$ and Hα/[S II] 6724 = 3.22) and PTP ($T(\mathrm{O}^{+2})/T(\mathrm{N}^{+}) = 1.13$ and Hα/[S II] 6724 = 3.74). Notice that higher temperature ratios are associated with lower values of Hα/[S II] 6724. In spite of these differences, the resulting total abundances (Table 4b) are very similar and typical of a type I PN, although a smaller helium abundance (0.157 vs. 0.162 in DU and 0.176 in PTP) and a higher nitrogen-to-oxygen abundance ratio (1.35 vs. 1.02 in DU and 0.93 in PTP) are found here (DU and PTP abundances were recalculated following the procedure used in this work). Notice that the minimum progenitor mass of type I PNe would have to be revised downwards if NGC 2818 is a cluster member. The central star temperature reported in Table 5 (149,000 K) is substantially smaller than the value derived from the He II 4686 intensity measured by DU and PTP, which is about 230,000 K. Central star temperatures are always lower than 230,000 K when the progenitor ZAMS mass is smaller than $3.0\,M_\odot$, and have this temperature in less than a thousand years (or after tens of thousands of years) if the mass is larger (VW94 and BL95). The spectra and overall appearence of NGC 2818 suggests that it is several thousand years old. If the central star temperature is closer to 149,000 K, models imply that the age of the PNN is between 3000 and 10,000 yr if the progenitor ZAMS mass is between 2.5 and $4\,M_\odot$ (VW94 and BL95). Larger masses lead to unreasonable age estimates.

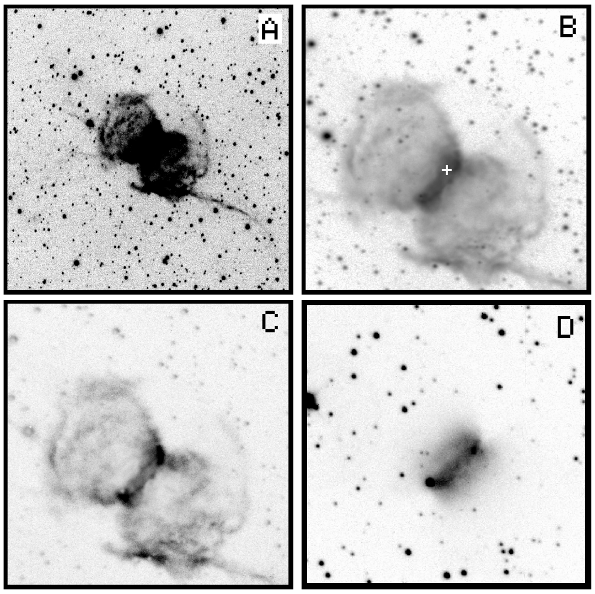

Fig. 15. Sh 1-89 in (*a*) [N II] 6584, (*b*) [N II] 6584 (logarithmic scale), (*c*) [N II] 6584/Hα, and (*d*) [O III] 5007. The position where the spectrum was taken is marked by a cross in *b*. The FOV is $470'' \times 470''$ in frame *a*, $256'' \times 256''$ in frames *b* and *c*, and $194'' \times 194''$ in frame *d*. North is up, east is to the left.

Images of NGC 2818 are presented in Figure 13: (*a*) [N II] 6584, (*b*) [N II] 6584/Hα, (*c*) *H2* (western side), and (*d*) [O III] 5007. The object is invisible in the *cK* frame, which implies that there is abundant shock excited emission from molecular hydrogen. The same conclusion has been established from infrared images of the eastern half (Schild 1995). Optical images suggest that NGC 2818 is an evolved bipolar PN, although the abundant and extensive emission of shocked H_2 implies that the object can not be too old. In the [N II] 6584 and [N II] 6584/Hα images the shell seems to burst-out to the NW and SE of the PN, in structures that appear to be point-symmetric. But notice that the NW structure can also be interpreted as the continuation of a string of bright condensations that goes accross the central cavity that is so clearly delineated in the [N II] 6584/Hα frame. In contrast with most bipolar type I PNe, there is no evidence of an inner ring of shocked H_2 confining the outflow. The segregation of regions with different excitation conditions is beautifully demonstrated in an RGB image of the western half of NGC 2818 (blue = [O III] 5007, green = [N II] 6584, and red = H_2), which is displayed in Figure 14.

m) Sh 1-89 The region in Sh 1-89 where the spectrum reported in Table 2c was taken is moderately excited, optically thick ([O II] 3727 and [O I] 6300 are intense) and possibly unaffected by shocks (Hα/[S II] 6724 = 3.44 and $T(\mathrm{O}^{+2})/T(\mathrm{N}^{+}) = 1.13$). He/H and N/O are typical of a type I PN (Table 4b). Notice that there is a very large amount of neon, about 3 times the average value found in this kind of planetaries (Peimbert 1990; KB), which implies that third dredge-up episodes probably occured during the final stages of the AGB phase. If so, a somewhat massive ZAMS progenitor produced this PN. The Zanstra temperature, which should be close to the PNN effective temperature in this optically thick object, is not too large (135,000 K, Table 5). This suggests that Sh 1-89 is an evolved object, in accordance with its physical appearence. According to evolutionary models for a $3.5\,M_{\odot}$ (VW94) and $4.0\,M_{\odot}$ (BL95), this is the temperature of the PNN after 10,000 to 15,000 yr, when its luminosity is close to $100\,L_{\odot}$. In models with more massive progenitors the PNN has this temperature very early on or after 100,000 yr, when there is no longer a visible PN.

The following set of images of Sh 1-89 are shown in Figure 15: (*a*) [N II] 6584, (*b*) [N II] 6584 (logarithmic scale), (*c*) [N II] 6584/Hα and, (*d*) [O III] 5007. The most interesting and mystifying features are the long quasi-filamentary structures that extend to the NE and SW in the light of [N II] 6584 (frame a). The tip of the SW structure is about $240''$ away from the geometrical center of Sh 1-89 and is $\sim 13''$ wide where it meets the main body of the nebula, i.e., 4.2 to 2.2 pc away from the center and 0.22 to 0.12 pc wide at a distance between 3.6 and 1.9 kpc (Zhang 1995). Both structures emerge from the main body of the nebula and neither of them points to the position where the PNN probably is (frame *b*), though it is not unthinkable that there were inner extensions that have been obliterated by the main ejection. Notice too that these structures are not mirror images of each other. Thus, there is no evidence suggesting that these structures were produced by a direct ejection from the central star, which would be the simplest solution to explain their existence. The hydrodynamical problem is confused even further by an additional bipolar structure (very conspicuous to the west) surrounding the principal nebular body. In addition, there is abundant and apparently isolated faint diffuse [N II] 6584 emission throughout the field. All these structures are much fainter or invisible in Hα, which implies that this material is not from the environment but was ejected by Sh 1-89 and is excited either by shocks or by the radiation field of the central star. The central ring confining the outflow is well defined in the [N II] 6584/Hα image (frame *c*) and less so when the object is seen in the light of [O III] 5007, where it is much more confined. As shown by KWGMP, shock-excited molecular emission is also concentrated in the central ring.

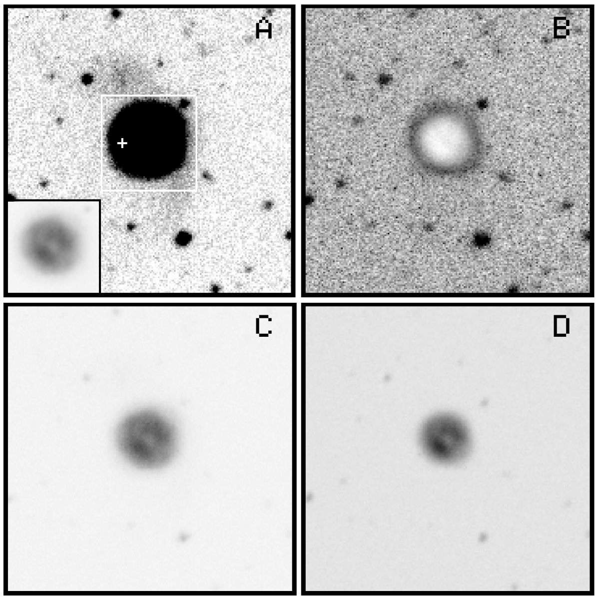

Fig. 16. Wray 16-22 in (*a*) Hα, (*b*) [N II] 6584/Hα, (*c*) Hα/Hβ, and (*d*) [O III] 5007/Hβ. The position where the spectrum was taken is marked by a cross in *a*. The FOV is $90'' \times 90''$ in all frames and $30'' \times 30''$ in the *a* sub-frame. North is up, east is to the left.

n) Wray 16-22 This is the only object in the sample where $T(\mathrm{O}^{+2})/T(\mathrm{N}^{+}) < 1$. Since these temperatures differ very little (Table 3), ion abundances (Table 4b) were determined assuming a uniform temperature equal to 12,700 K, which is the mean value of $T(\mathrm{O}^{+2})$ and $T(\mathrm{N}^{+})$. Wray 16-22 is found to be deficient in helium and its overall chemical composition suggests it is a type III PN, which probably are the end product of population II stars. As such, a low mass ZAMS precursor is expected. This is substantiated by the Zanstra temperature (103,000 K, Table 5), which is characteristic of the less massive PNN produced by low-mass stars. From this temperature and the evolutionary tracks of VW94 it follows that the ZAMS mass was between 1.0 and $1.5\,M_{\odot}$, that the star formed between 0.4 and 1.5×10^{10} yr ago and that the PN is about 10,000 yr old.

Images of Wray 16-22 are displayed in Figure 16: (*a*) Hα, (*b*) [N II] 6584/Hα, (*c*) Hα/Hβ, and (*d*) [O III] 5007/Hβ. The nebula is confined by a low excitation nearly circular ring apparent in frame *b*.

Most of the [O III] 5007 emission is within this structure (frame *d*). The Hα/Hβ line ratio (frame *c*) is nearly constant, which implies an almost uniform extinction for the nebula. The most interesting feature in these images is the low emission arc (convex to the NW) seen in the Hα frame. It can be interpreted as a bow shock produced by the supersonic motion of Wray 16-22 (towards the NW) with respect to the interstellar medium. If so, the object is moving away from the galactic plane.

4. CONCLUSIONS

1. The two primary criteria (He/H ≥ 0.125 and N/O ≥ 0.5) defining type I PNe are fulfilled in A 14, A 24, A 79, K 3-46, K 3-91, M 1-28, M 1-57, M 3-3, M 3-5, NGC 2818, and Sh 1-89. Objects exhibiting shocked molecular hydrogen are A 79, K 3-46, K 3-91, M 1-28, M 3-3, probably M 3-5, NGC 2818, and Sh 1-89. In all cases H_2 was found to be close to the region where [N II] 6584 emission is brighter, though slightly further away from the geometrical center, as predicted by models of H_2 formation in PNe (Guerra Aleman 2002). This stratification is clearly seen in an RGB image of NGC 2818 (Figure 14).

2. Shock excited H_2 was not found in type I PNe A 14, A 24, and M 1-57. Two of these are evolved objects (A 14 and A 24), but the spectroscopic and imaging data for M 1-57 indicates that it is a young PN. Thus, the existence of shock-excited molecular hydrogen is not only related to the progenitor mass (i.e., the ejected mass), but also to the evolutionary stage of at least some type I planetary nebulae. The absence of molecular hydrogen in M 1-57 is in contradiction with models predicting a larger amount of H_2 in hotter stars (Guerra Aleman 2002).

3. The neon abundance of A 24, A 79, M 1-57, and Sh 1-89 suggests that third dredge-up episodes occured in their progenitor stars. N/O and specially He/H are very large in A 24 and A 79 (Table 5). It is worth noticing that the central star temperature is not too high in any of these objects.

4. Large $T(\mathrm{O}^{+2})/T(\mathrm{N}^{+})$ ratios combined with small values for Hα/[S II] 6724 were observed in A 79, M 1-28, and NGC 2818 (see Table 5). This combination was interpreted by BJ as evidence for the presence of shock waves in the inspected regions. Shock excitation is also suspected in A 14, A 24, and K 3-46, though the temperature ratio could not be determined.

5. Images of Hα/Hβ show that extinction is asymmetric in M 1-57, M 3-3, and M 3-5. This peculiarity was also found in NGC 6302 (Bohigas 1994), where it was established that it is due to local and as yet unexplained conditions.

6. Filamentary structures pointing towards the central star were discovered in a [N II] 6584/Hα image of A 24. These can be explained by temperature variations not larger than $\sim 10\%$.

7. DeHt 3 is a type II PN with a He abundance that is more common in type I PN, a situation that has also been found in other planetary nebulae (BJ and KB).

8. KjPn 6 is a bipolar planetary nebula with a nitrogen-to-oxygen abundance ratio (1.38) indicative of a massive progenitor. Other properties of this object, such as its low helium, nitrogen and oxygen abundances, the absence of molecular hydrogen emission and the low temperature of the central star suggest otherwise. The nature of this object is confused even further by the fact that it is at least 800 pc above the Galactic plane. It is suggested that KjPn 6 may be a type I PN produced by a star formed in a high latitude low metallicity molecular region.

9. In this sample it is certain that the extremely long off-centered quasi-filamentary [N II] 6584 structures in Sh 1-89 present the most interesting challenge for HD and MHD models for the structure of planetary nebulae. These are not mirror images of each other. The filaments are much fainter in Hα, which implies that they are formed by material ejected by the central star and are not excited by an external source.

10. An emission arc in the NW edge of Wray 16-22 is interpreted as a possible bow shock produced by the supersonic motion of this object with respect to the interstellar medium.

The author is grateful for the excellent assistance provided by the staff of San Pedro Mártir and the valuable comments given by an unknown referee. Partial support from DGAPA-UNAM project IN-105400 is acknowledged.

REFERENCES

Acker, A., James, M., Ochsenbein, F., Stenholm, B., & Tylenda, R. 1992, Strasbourg-ESO Catalogue of Planetary Nebulae

Acker, A., Köpen, J., Stenholm, B., & Jasniewicz, G. 1989, A&AS, 80, 201 (AKSJ)

Acker, A., Köpen, J., Stenholm, B. & Raytchev, B. 1991, A&AS, 89, 237 (AKSR)

Aller, L. H. 1984, Physics of Thermal Gaseous Nebula, (Dordrecht: Reidel)

Blöcker, T. 1995, A&A, 299, 755 (BL95)

Bohigas, J. 1990, Reporte Técnico No. 92, Inst. de Astronomía, UNAM

———. 1994, A&A, 288, 617
———. 2001, RevMexAA, 37, 237 (BJ)
Bohigas, J., & Tapia, M. 2003, AJ, submitted
Cruz-González, I., Carrasco, L., Ruiz, E., et al. 1994, Proc. of SPIE, Astronomical Instrumentation, 8, 199
Chini, R., & Wink, J. E. 1984, A&A, 139, L5
Dufour, R.J. 1984, ApJ, 287, 341 (DU)
Guerra Aleman, I.R. 2002, M.Sc. Thesis, IAG, Universidade de São Paulo
Hua, C. T., & Kwok, S. 1999, A&AS, 138, 275
Hua, C. T., & Martinis, J. 2002, Ap&SS, 281, 777
Iben, I. 1995, Phys. Reports, 250, 1
Kaler, J. B. 1986, ApJ, 308, 322
Kaler, J. B., & Jacoby, G. H. 1989, ApJ, 345, 871
Kaler, J. B., Kwitter, K. B., Shaw, R. A., & Browning, L. 1996, PASP, 108, 980 (KKSB)
Kaler, J. B., Shaw, R. A., & Kwitter, K. B. 1990, ApJ, 359, 392 (KSK)
Kastner, J. H., Weintraub, D. A., Gatley, I., Merrill, K. M., &, Probst, G. 1996, ApJ, 462, 777 (KWGMP)
Kazarian, M. A., Parsamian, E. S., & Parrao, L. 1998, Astrophys., 41, 239 (KPP)
Kingdon, J., & Ferland, G. J. 1995, ApJ, 442, 714
Kingsburgh, R., & Barlow, M. J. 1994, MNRAS, 271, 257 (KB)
Manchado, A., Guerrero, M. A., Stanghellini, L., & Serra-Ricart, M. 1996, The IAC Morphological Catalog of Northern Galactic Planetary Nebulae, Instituto de Astrofísica de Canarias (IAC-Catalog)
Mermilliod, J.-C., Clariá, J. J., Andersen, J., Piatti, A. E., & Mayor, M. 2001, A&A, 375, 30
Milingo, J. B., Henry, R. B.C ., & Kwitter, K. B. 2002, ApJS, 138, 285
Milingo, J. B., Kwitter, K. B., Henry, R. B. C., & Cohen, R. E. 2002, ApJS, 138, 279 (MKHC)
Pedreros, M. 1989, AJ, 98, 2146
Peimbert, M. 1990, Rep. Prog. Phys., 53, 1559
Peimbert, M., & Torres-Peimbert, S. 1983, in IAU Symp. 103, Planetary Nebulae, ed. D. R. Flower, (Dordrecht: Reidel), 233
———. 1987, RevMexAA, 14, 540 (PTP)
Phillips, J. P., & Cuesta, L. 1998, A&AS, 133, 381
Rodríguez, M., Corradi, R. L. M., & Mampaso, A. 2001, A&A, 377, 1042 (RCM)
Sabbadin, F., Falomo, R., & Ortolani, S. 1987, A&AS67, 541, (SFO)
Schild, H. 1995, A&A, 297, 246
Seaton, M. J. 1979, MNRAS, 187, 73P
Tifft, W. G., Connolly, L. P., & Webb, D. F. 1972, MNRAS, 158, 47
Vassiliadis, E., & Wood, P. R. 1994, ApJS, 92, 125 (VW94)
Zazueta, S., et al. 2000, RevMexAA, 36, 141
Zhang, C. Y. 1995, ApJS, 98, 659

Joaquín Bohigas: Instituto de Astronomía, UNAM, Carretera Tijuana-Ensenada Km 103m 22860 Ensenada, B. C., México (jbb@astrosen.unam.mx).